Optimization Algorithm for Antenna Impedance Matching in Digitally Tunable Network

by

Sung Eun Kim

A thesis

presented to the University of Waterloo

in fulfilment of the

thesis requirement for the degree of

Master of Applied Science

in

Electrical and Computer Engineering

Waterloo, Ontario, Canada, 2015

© Sung Eun Kim 2015

Author’s Declaration

I hereby declare that I am the sole author of this thesis.

This is a true copy of the thesis, including any required final revisions, as accepted by my examiners.

I understand that my thesis may be made electronically available to the public.

Abstract

In this work, we explore different methods to tune the antenna impedance in mobile devices. Mismatch from antenna impedance can cause undesirable effects such as spurious emissions, channel leakages, increased noise floor, degraded receiver sensitivity and so on.

With the advancement in technology, digitally tunable reactive components are now available. Thus, a feedback system with tunable circuitry and the aperture tuning method where the component is directly embedded in the antenna design are some of the popular choices of solution.

The 'look-up table' method is currently widely adopted in wireless industry. The hardware component chain (RF chain) contains the set-up to measure Γ_{in} (ratio of reflected signal to transmitted signal in dB) and a circuit to be tuned according to the values found in the look-up table. The look-up table is a pre-defined calibration chart provided by the manufacturer. It is saved in the memory of the device for permanent use during its lifespan.

In this thesis, in the effort to eliminate the process of creating this look-up table and also to free up large space of memory, we approach an analytical solution to predict the exact values of the component in the tunable circuit – hence, making the procedure a one-time measurement, so called the open-loop configuration.

In Chapter 3, a thorough mathematical analysis has been developed to integrate the Q factors of each component into a sample pi-circuit. In such setup, the system is expected to calculate Z_L (or the antenna, load) with measured Γ_{in} and then compute the three capacitance values that yield the best transducer gain by conjugate matching method. However, due to many non-ideal characteristics of the components, calibrating the setup and incorporating the calibration data into analytical solution becomes very challenging.

Therefore, the closed-loop configuration is more useful. It collects the empirical data of Γ_{in}, apply the optimization algorithm and then tune the circuitry in feedback manner, until the lowest desired Γ_{in} is reached. (Note that there is no difference between the closed and open loop configuration in the physical set-up.)

The purpose of this thesis is to develop the optimization algorithm used in closed-loop configuration. It involves three degrees of freedom using three Digitally Tunable Capacitors (DTCs). Accordingly, the challenge of this research points to inventing a 3D-unconstrained optimization technique that is simple enough to be implemented in a microprocessor without employing complex equation-solving libraries.

In Chapter 4, the Hill-Climbing algorithm is investigated to see if it provides a suitable approach for finding the global minimum Γ_{in} in the 3D space gradient defined by 3 variables or DTCs. The Hill Climbing method, however, will limit its solution to finding only the local minimum within the gradient. This means that the location of the solution will change with the resolution of the gradient and the search step-size. Therefore,it is expected that Hill Climbing algorithm yields different solutions depending on the increment size and the starting location of the search.

Chapter 5 develops a new algorithm that is based on Grid Searching. The main idea is to grasp the picture of the entire gradient of 3D space and zoom-in closer to the global point by iteration. The challenge lies in defining the boundary of zoom-in region without leaking the global point and leaving it behind. Also, the scanning of the reduced region in each iteration must not be too rigorous – meaning requiring too many data points.

All different pi-network will have its limited coverage region on Smith Chart, of which the load impedance can be matched with. Therefore, selecting the reactive component with the suitable range of capacitance is also an important step, in order to fully utilize the work of this thesis. Apart from that, the algorithm does not require any information about the antenna, frequency of operation nor the configuration of the DTCs.

Overcoming these challenges will guarantee the device to have the best optimized state of impedance match, at a specific frequency. Given that the algorithm is a 3D optimization technique, the work of this research does not only apply to tuning a pi-tuner. The three DTCs can be also integrated in the aperture tuning system.

Thesis Supervisor: Professor Safieddin Safavi-Naeini.

Acknowledgements

I would like to express my sincere appreciation to my advisor, Prof. Safieddin Safavi-Naeini, without whose guidance, this thesis would not be possible. Professor Safavi's love of research, intuition and care for his team members are something special we see. He has given me an unconditional trust and support which define me today.

Many thanks to our ISTP members: Dr. Mohammad-Reza Nezhad-Ahmadi and Dr. George Shaker for supervising us (me and Zhichao) by holding valuable meetings every week. We always look up to them and felt so lucky to have these two great mentors.

I would like to thank my co-op manager, Mr. Muresan, who brought me to the field of RF engineering. His values and advices will continue to remain in me.

A special thanks to my fellow graduate students: Zhichao, Stanley and our antenna course TA: Behrooz for their academic support and friendship through shared graduate experience. Thank you to Maryam and Kyung Eun, my housemate, for making me feel at home. Thank you to all my old friends from undergrad, Dominic, Jack, Min, Jiewon, Steven and Brian, majority of whom are now in Silicon Valley, launching the first step in their career. Good luck to all my friends.

Finally, I would like to thank my parents for always standing behind me with your love.

This thesis is dedicated to my Mom and Dad.

Table of Contents

List of Figures

List of Tables

Chapter 1

1 Introduction

As an introduction, we briefly explore the available options of antenna impedance matching in wireless devices and realize that digitally tunable capacitors (DTCs) are useful in creating a tunable circuit system that can also adopt a searching algorithm.

Such network, whether it is a tunable circuit or aperture tuning system, will require a method to determine the values for the components. Largely available is the look-up table method, where manufacturers store all the states of matched solutions in the memory.

In this thesis, we develop an alternative to this look-up table solution – an algorithm that optimizes the matching by finding the ultimate values of capacitors from empirical data points.

1.1 Impedance Matching Methods

Impedance matching, in general, can be achieved by a variety of methods: lumped circuit (L, T, ∏), single and double stub tuning with either open or short ends, quarter wave transformer ($Z_{transformer} = \sqrt{Z_o Z_L}$) and multisection matching transformers for broader bandwidth applications. [1]

1.1.1 Lumped Circuit Network

Tunable components can be attached at the antenna input in shunt or series, providing an easy solution for impedance tuning. Such lumped circuit recently became realizable thesedays, by the introduction of tunable capacitors due to advancement in fabrication technology. There are three main technologies used to develop tunable impedance matching network – Micro-Electromechanical systems (MEMs) capacitors, Barium Strontium Titanate (BST) capacitors and Digitally Tunable Capacitors (DTCs).

MEMS capacitors have two plates that change its separation for the required value of capacitance in tunable network. [2][3] BST technology is used with high DC voltage bias with thin-film ferro-electric materials. [4] In this thesis, we use DTCs. DTCs are controlled by digital signals and it makes the Serial Peripheral Interface (SPI) connection easy to implement between the microprocessor.

1.1.2 Binary Capacitance Array

Binary capacitance array is a cheap and easy way to implement using fixed values of capacitance. There are discrete steps of capacitance values that are engaged by switches, but the drawback is that the impedance range is quite limited. [5]

1.1.3 Aperture Tuning

Aperture tuning is adding a tunable component in the antenna structure itself. It changes the electrical length of the antenna and shifts the frequency band. DTCs are suitable for such application. However, the added component should have low loss to not interfere with the radiation efficiency of the antenna. [6]

1.2 Impedance Matching Theory

Mismatch from antenna impedance can cause severe effect on the power amplifier. [7] Spurious emissions and channel leakages are the examples. Also, with increased noise floor, the receiver sensitivity is largely degraded. [8] This section covers the fundamentals of impedance matching theory.

Impedance matching circuit is a *reciprocal* and *symmetric* network defined by the fundamentals of RF theory. For an arbitrary N-port network, one can characterize the network with $V_n = V_n^+ + V_n^-$ and $I_n = I_n^+ - I_n^-$ for total voltage and total currents of all terminals. [1] The voltages and currents are related by the impedance matrix such that,

$$[V] = [Z][I] \qquad (1)$$

The network is **reciprocal** if it does not contain any active devices and contains only isotropic materials. Cables, attenuators, couplers and power splitters are all the examples of reciprocal network. In a reciprocal network, the scattering parameters reflect power losses between any two ports regardless of direction of propagation. (*i.e.*, $S_{12}=S_{21}$ and $S_{13}=S_{31}$) Therefore, the impedance and admittance matrices for reciprocal network are ideally symmetric. [1]

If the network is lossless, the summed output power at all ports reflect the incident power at one port. If the network is an active device, power is added to the output, so the network cannot be called lossless. For lossless network, the real part of impedance matrix is zero and scattering matrix is unitary. [1]

$$[S] = [S]^t \qquad (2)$$

$$[S][S]^{*t} = [U] \qquad (3)$$

In this regard, a matched network, as a whole, has all ports matched to the same impedance, Z_o=50 Ω, making the diagonal S parameters (*i.e.*, S_{11}, S_{22}, …) zero, making the reflection coefficient zero as well.

The lumped circuit matching network can be referred to as a passive device, abiding to two properties – reciprocal and lossless. However, matching network is not impedance matched by itself. The design goal of matching network is so that the impedance looking into one port while a load impedance is at the other end will be 50 ohms (=Z_o).

1.3 Conjugate Matching and Maximum Power Transfer

With an ideal, lossless transmission line, the average power is defined by (4) when the source has impedance $Z_g = R_g + jX_g$ and load has impedance $Z_{in} = R_{in} + jX_{in}$. [1]

$$P = \frac{1}{2} Re\{V_{in} I_{in}^*\} = \frac{1}{2} |V_g|^2 \frac{R_{in}}{(R_{in} + R_g)^2 + (X_{in} + X_g)^2} \quad (4)$$

From a fixed power source, conjugate matching of the load Z_{in} (5) to internal generator impedance Z_g gives the maximum power transfer to the load (6). [1]

$$Z_{in} = Z_g^* \ (R_{in} = R_g \ and \ X_{in} = -X_g) \quad (5)$$

$$P = \frac{1}{2} |V_g|^2 \frac{1}{4R_g} \quad (6)$$

Note that, Γ_{in} is not necessarily zero unless Z_g is real. ($ie. Z_g = Z_o = 50\Omega$)

$$\Gamma_{\text{in}} = \frac{Z_{in} - Z_g}{Z_{in} + Z_g} = \begin{cases} 0, & Z_g \ is \ real \\ not \ 0, & Z_g \ is \ not \ real \end{cases} \quad (7)$$

From the definition of average (real) power, P_{in} delivered for the network from the source can be derived as,

$$P_{in} = \frac{|V_S|^2}{8Z_o} \frac{|1 - \Gamma_S|^2}{|1 - \Gamma_S \Gamma_{in}|^2} (1 - |\Gamma_{\text{in}}|^2) \quad (8)$$

When we insert a two port network with [S] matrix at the antenna input as shown in Figure 1-1, the power delivered to the load is defined by (9).

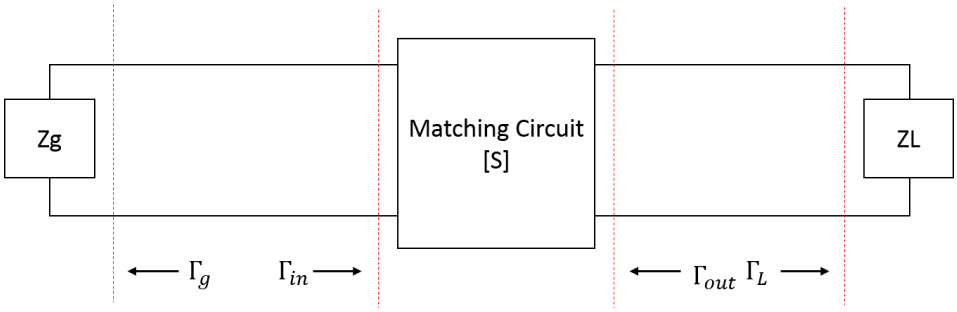

FIGURE 1-1: A TWO-PORT NETWORK WITH SOURCE AND LOAD IMPEDANCE

$$P_L = \frac{|V_S|^2}{8Zo}\frac{|S_{21}|^2(1-|\Gamma_L|^2)|1-\Gamma_S|^2}{|1-S_{22}\Gamma_L|^2|1-\Gamma_S\Gamma_{in}|^2} \qquad (9)$$

Then, the ratio of the power dissipated in the load (9) and the average power input to the system (8) can be expressed as power gain G such that,

$$G = \frac{P_L}{P_{in}} = \frac{|S_{21}|^2(1-|\Gamma_L|^2)}{(1-|\Gamma_{in}|^2)|1-S_{22}\Gamma_L|^2} \qquad (10)$$

Note that the power available for the network can be maximized from P_{in} when the source impedance Γ_S is matched to Γ_{in} such that $\Gamma_{in} = \Gamma_S^*$.

Also, the power delivery from the output at the two-port network to the load can be maximized when load impedance, Γ_L, is matched to Γ_{out} such that $\Gamma_L = \Gamma_{out}^*$. [1]

Depending on which junction(s) is matched, the power gain is also redefined accordingly. For instance, when $\Gamma_{in} = \Gamma_S^*$, the ratio of power dissipated by the load and the power available for the network is defined by (11) and is called transducer gain. [1]

$$G_T = \frac{P_L}{P_{for\ network}} = \frac{|S_{21}|^2(1-|\Gamma_S|^2)(1-|\Gamma_L|^2)}{|1-\Gamma_S\Gamma_{in}|^2\ \ |1-S_{22}\Gamma_L|^2} \qquad (11)$$

Note how the term $|\Gamma_{in}|^2$ changed to $\Gamma_s\Gamma_{in}$ from (10). Also, (11) becomes $G_T = |S_{21}|^2$ when $\Gamma_S = \Gamma_L = 0$.

1.4 Matching Network Topologies

With the advancement in technology, DTCs enable lumped circuit as an option for impedance matching method in higher frequencies. Depending on the topology, perfect conjugate match can be obtained by matching $Z_{in} = Z_g^*$ where resistance of both sides are equal and imaginary parts are opposite in sign.

Two possible L network configurations are shown in Figure 1-2, for separate cases of $R_L > R_o$ and $R_L < R_o$. These two configurations of L-type network are capable of conjugate matching on limited region on the Smith Chart. [9] The reactive elements in lumped circuit topologies can be either capacitors or inductors. When the range of the component is limited, the conjugate matching can only be achieved as long as the load is located within the matching domain on Smith Chart. [10]

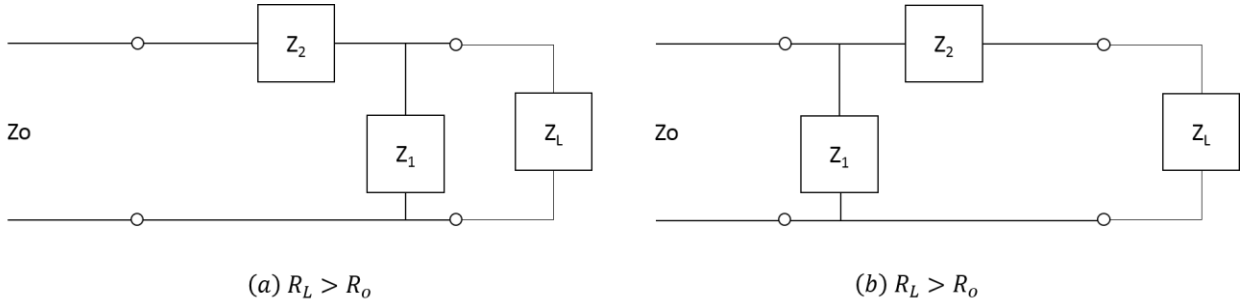

$(a)\ R_L > R_o$ $(b)\ R_L > R_o$

FIGURE 1-2: TWO POSSIBLE L NETWORK CONFIGURATIONS

There is a chance of antenna impedance varying between the two cases when the hardware is developed on one configuration - resulting in no match. To save such risk, Pi- or T- network, as shown in Figure 1-3, can be used [11]. These networks can transform into either of (a) or (b) in Figure 1-2 by turning off a branch. It would be necessary that each of the three branches has a tunable component (DTC) to grant three degrees of freedom in total.

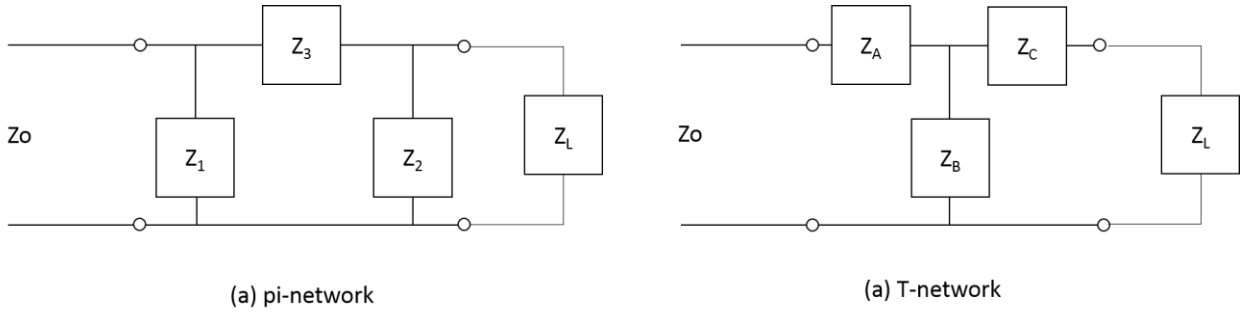

(a) pi-network (a) T-network

FIGURE 1-3: PI-NETWORK AND T-NETWORK

Computing the analytical solution for reactive components in Pi- and T- network is a much more complex exercise compared to L network. To find solutions where the source and load are in perfect conjugate match, the network has to be divided into source and load side as shown in Figure 1-4. [12]

Upon a match, a common intermediate resistance will exist between the two sides in the analytical solution. This means that there are always more than one solution to impedance matching using Pi- or T-network.

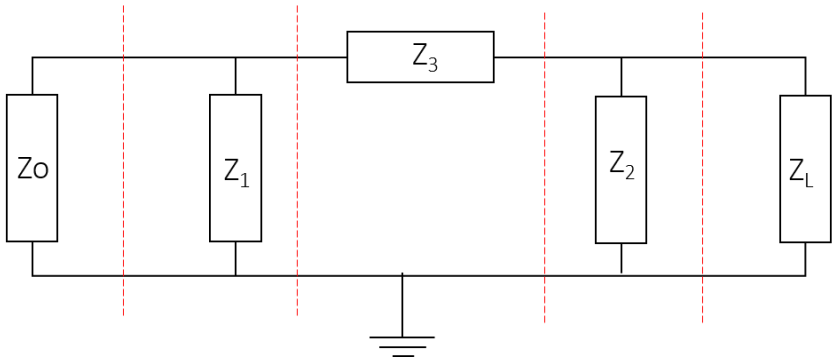

FIGURE 1-4: DIFFERENT WAYS TO DIVIDE PI-NETWORK INTO SOURCE AND LOAD SIDE

It is important to note that each set of solutions has different quality factor, bandwidth and power gain and transducer gain. [13]

Chapter 2

2 Implementation

2.1 Building Blocks

In this section, we discuss each building block in hardware setup for lumped circuit antenna impedance measurement and tuning as shown in Figure 2-1. It is similar to the closed look configuration found in [14].

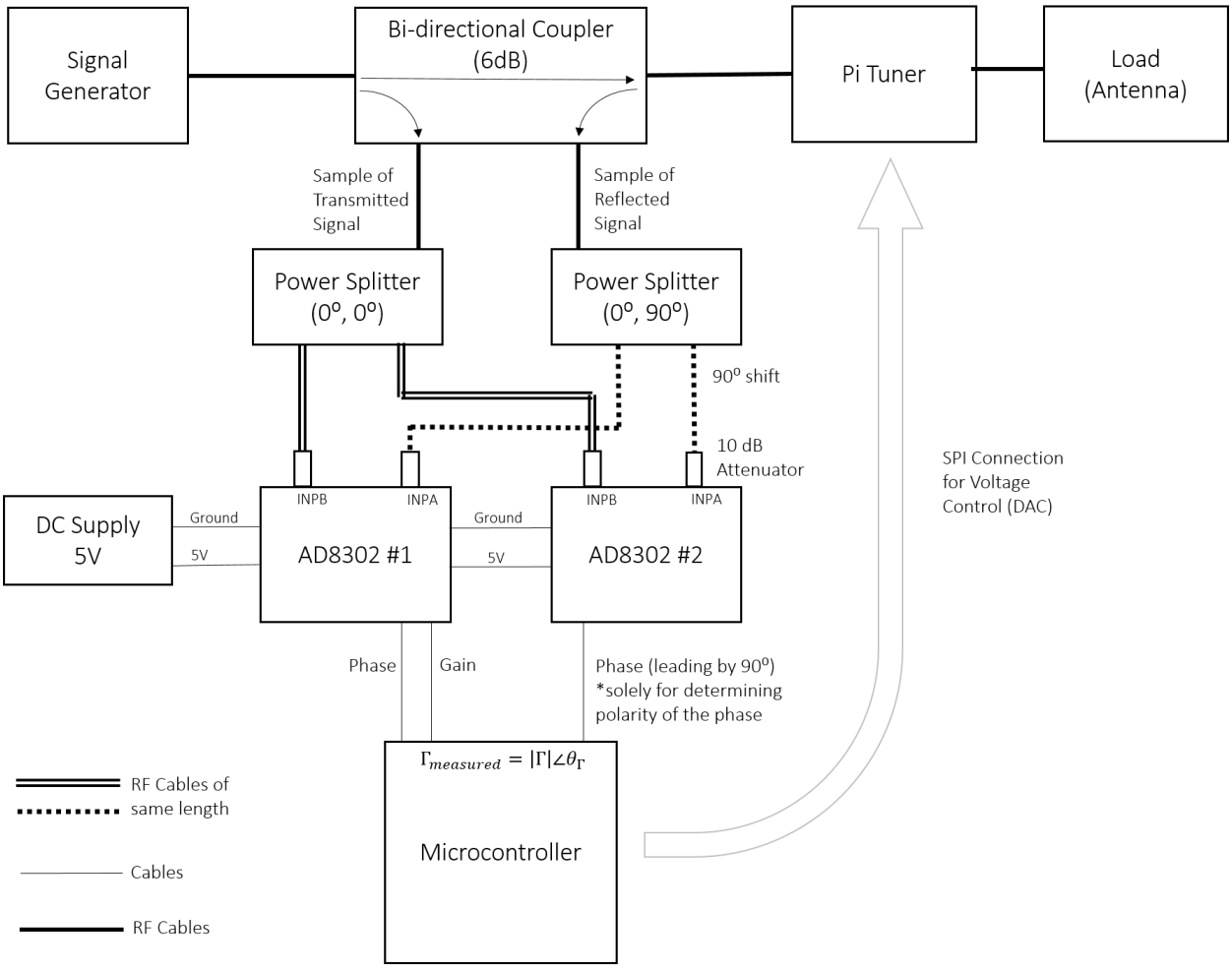

FIGURE 2-1: TUNABLE IMPEDANCE MATCHING NETWORK WITH TWO AD8302 FOR PHASE AND MAGNITUDE MEASUREMENT.

2.1.1 Adaptive Tuner

We have used a pi-circuit implemented on a PCB board with digital and RF circuitry, attached with two RF ports. The board has a main RF transmission line serving as the spine of pi-circuit and its EM effect with the PCB adds to non-idealness in analytical prediction for the result, as seen in the next chapter.

Also, the pi-tuner has Serial Peripheral Interface (SPI) that allows the microcontroller to communicate with each of the DTCs digitally. The microcontroller and the tuner board will be connected by five ports: SCLK, MOSI, MISO, SS and ground for sending the address of each capacitor and the required voltage level in timely synchronized manner according to the algorithm.

2.1.2 Digitally Tunable Capacitors

We have used On-Semiconductor's DTCs for our experiment. DTCs thesedays provide a high quality factor and is therefore very suitable for dynamic adjustment for antenna impedance matching system [15] and also is easy to implement for SPI. The DTCs are provided with a datasheet presenting its capacitance vs. voltage graph, as shown in Figure 2-2 as a sample.

It is important to note that the voltage applied to the capacitor does not have a linear correspondence to the capacitance. In fact, the capacitance and voltage graph has variation due to factors such as temperature, therefore it is not possible to achieve accurate capacitance by applying the required voltage calculated from one best-fit polynomial equation.

Also, charging time at very low voltage near zero is extremely slow in DTCs. Therefore, it is normally a good practice to only use the region excluding very low voltage around 0~2 V.

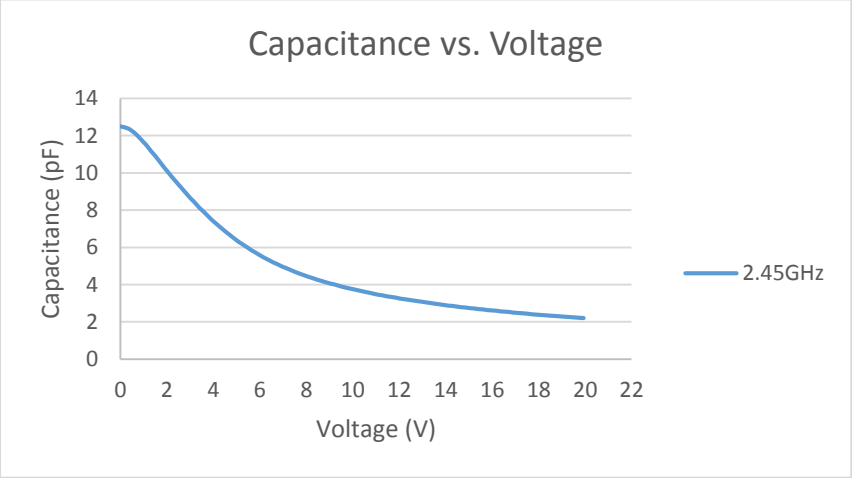

FIGURE 2-2: SAMPLE CAPACITANCE VS. VOLTAGE GRAPH FOR 8.2 PF DTC (Q=70, F=2.45GHZ)

2.1.3 Magnitude and Phase Detector (AD8302)

The Voltage Standing Wave Ratio (VSWR) and Return Loss (Γ_{in}) are the most important parameters to be investigated for trouble-shooting and repair in impedance matching. AD8302 by Analog Design is the leading component in Gain and Phase Detection and can be used to detect the magnitude and phase of the reflection coefficient. There are two constraints proposed in AD8302.

Firstly, for the phase measurement, the difference between two input signals for an AD8302 could range from -180 to 180 degrees. However, AD8302 output – in voltage – does not provide information about the sign of the phase difference. For example, if the output of AD8302 is 0.9V for 90 degrees, it is unknown whether the result is +90 degrees or -90 degrees. In order to overcome this, we deploy two AD8302s as shown in Figure 2-1 introduced in [16].

The sample *transmitted* signal from signal generator is fed into AD8302 #1 and #2 and the sample *reflected* signal from the antenna input is also fed into both #1 and #2 – but with +90 degree shift applied on #2. This is done by phase splitter with 0 and 90 degree phase difference as shown in Figure 2-1. AD8302 #2 therefore serve as a reference to AD8302 #1 for the sign of the result. [16]

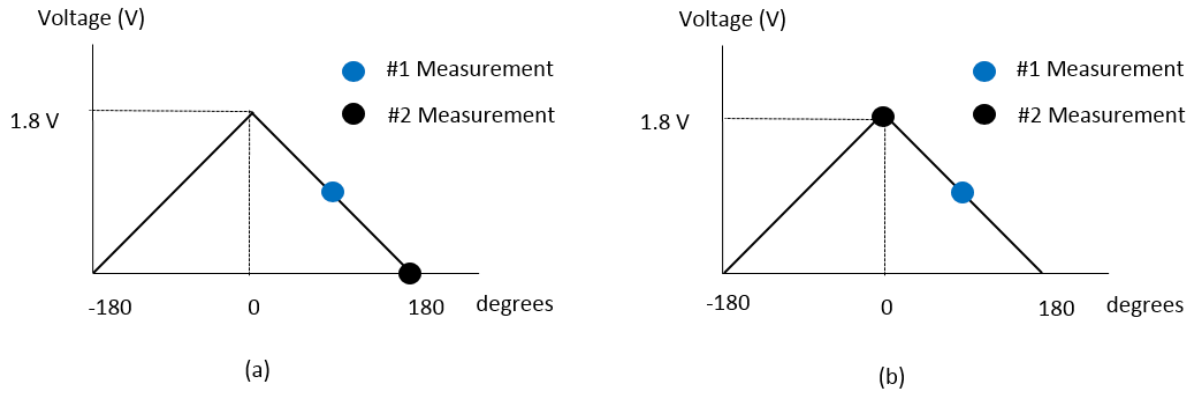

FIGURE 2-3: METHOD FOR DETECTING SIGN OF PHASE USING TWO AD8302

If we assume that the input paths for these two AD8302 ideally has the same path loss, disregarding the coupler, the phase reading from AD8302 #2 will be exactly +90 degrees apart from AD8302 #1. As shown in Figure 2-3, if AD8302 #1 reads 90 degrees and AD8302 #2 reads 180 degrees, we know that it is +90 degrees. Or, if AD8302 #2 reads 0 degree, then AD8302 #1 means -90 degrees. [17]

Secondly, for gain measurement, one of the two input signals has to be used as a reference measure at -30 dBm and the other signal can sweep between -60 dBm to 0 dBm to yield output in the range of -30 dB to 30 dB. Any deviation from -30 dBm of this reference signal will result in reducing the measurement range

for the second signal. If we define Input A as reflected signal strength and Input B as the transmitted signal strength, the output can be expressed as,

$$\text{Input A (dBm)} - \text{Input B (dBm)} = \text{Output (dB)} \qquad (12)$$

Thus, the exact loss of the set-up has to be measured and taken into account to regulate the input power level to deliver the signal to AD8302's Input B port at -30 dBm. [16]

2.2 Calibration

Section 2.1.3 indicates that the calibration for this setup, Figure 2-1, is complicated. With some assumptions, we can set up a calibration procedure for path loss according to Figure 2-4.

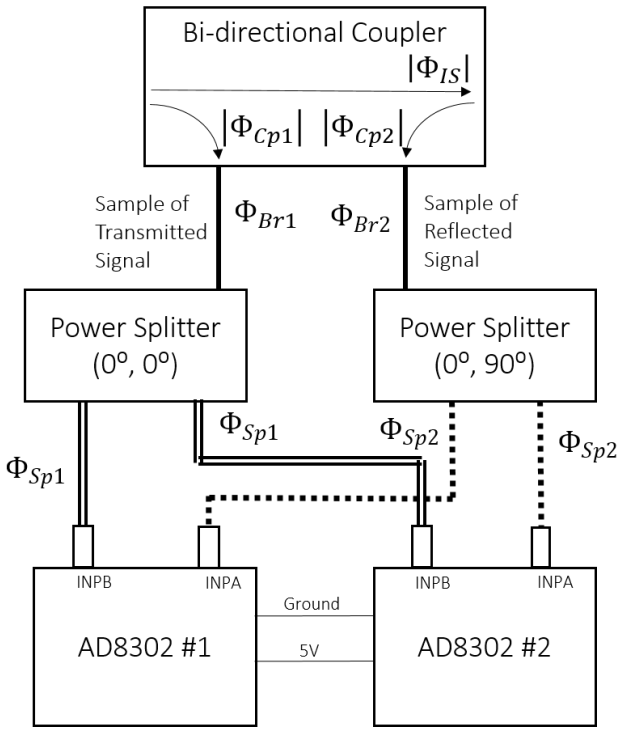

FIGURE 2-4: CALIBRATION FOR SETUP.

- Let the cable loss for branch 1 (left section of Figure 2-1) be $\Phi_{Br1} = |\Phi_{Br1}|\angle\theta_{Br1}$.
- Let the cable loss for branch 2 (right section of Figure 2-1) be $\Phi_{Br2} = |\Phi_{Br2}|\angle\theta_{Br2}$.
- Let the coupling for 6 dB coupler for transmitted signal side (left) and reflected signal side (right) be:
    - $\Phi_{Cp1} = |\Phi_{Cp1}|\angle\theta_{cp1} = 6(dB)\angle\theta_{coupling1}$ and
    - $\Phi_{Cp2} = |\Phi_{Cp2}|\angle\theta_{cp2} = |\Phi_{IS}|\angle\theta_{IS} + 6(dB)\angle\theta_{coupling2}$, where $|\Phi_{IS}|\angle\theta_{IS}$ is the insertion loss of the coupler.

- Let the impedance of pi tuner and load together be $\Phi_{Load} = |\Phi_{Load}|\angle\theta_{Load}$.
- Let the cable loss after power splitter for transmitted signal be
  - $\Phi_{Sp1} = |\Phi_{Sp1}|\angle\theta_{Sp1}\ and\ |\Phi_{Sp1}|\angle\theta_{Sp1}$ and
  - $\Phi_{Sp2} = |\Phi_{Sp2}|\angle\theta_{Sp2} = |\Phi_{Sp2}|\angle\theta_{Sp2}{}^{0} and\ |\Phi_{Sp2}|\angle\theta_{Sp2}{}^{0} + 90^{0}$

Then, we can define an equation for the transmitted and reflected signal.

$$|Transmitted| = Power\ Input - |\Phi_{Cp1}| - |\Phi_{Br1}| - |\Phi_{Sp1}| \tag{13}$$
$$|Transmitted| = Power\ Input - 6(dB) - |\Phi_{Br1}| - |\Phi_{Sp1}|$$

$$\begin{aligned} |Reflected| &= Power\ Input - |\Phi_{Cp2}| - |\Phi_{Load}| - |\Phi_{Br2}| - |\Phi_{Sp2}| \\ &= Power\ Input - |\Phi_{IS}| - 6(dB) - |\Phi_{Load}| - |\Phi_{Br2}| \\ &\quad - |\Phi_{Sp2}| \end{aligned} \tag{14}$$

Using (13) and (14), we can define the gain.

$$\begin{aligned} Gain, \Gamma_{\text{measured}}(dB) &= |Reflected| - |Transmitted| \\ &= \{-|\Phi_{Br1}| - |\Phi_{Sp1}| - |\Phi_{Load}|\} - \{-|\Phi_{IS}| - |\Phi_{Br2}| - |\Phi_{Sp2}|\} \\ Gain &\approx -|\Phi_{Load}| - |\Phi_{IS}| \end{aligned} \tag{15}$$

For phase measurements,

$$\angle\theta_{\Gamma1(\text{measured})} = \angle\Phi_{reflected} - \angle\Phi_{Transmitted} \tag{16}$$

$$\angle\theta_{\Gamma1(\text{measured})} = \{\angle\theta_{IS} + \angle\theta_{coupling2} + \angle\theta_{Br2} + \angle\theta_{Sp2} + \angle\theta_{Load}\} - \{\angle\theta_{Coupling1} + \angle\theta_{Br1} + \angle\theta_{Sp1}\} \tag{17}$$

$$\angle\theta_{\Gamma2(\text{measured})} = \angle\Phi_{reflected} + 90^{0} - \angle\Phi_{Transmitted} \tag{18}$$

$$\angle\theta_{\Gamma2(\text{measured})} - \angle\theta_{\Gamma1(\text{measured})} = +90^{0}(leading) \tag{19}$$

$$\angle\theta_{\text{Load}} = \angle\theta_{\Gamma1(\text{measured})} - \{\angle\theta_{IS} + \angle\theta_{coupling2} + \angle\theta_{Br2} + \angle\theta_{Sp2}\} + \{\angle\theta_{Coupling1} + \angle\theta_{Br1} + \angle\theta_{Sp1}\} \tag{20}$$

For magnitude measurement, the two branches for transmitted and reflected signal samples after the coupler, including 6-dB coupling loss for both sides, have almost the same path loss using the same cables. The remaining causes for the difference between transmitted and reflected signal are the insertion loss of the coupler $|\Phi_{IS}|$ and the load. Thus, we get a very simple equation to find Γ_{Load} with Γ_{measured}.

The phase measurement is usually a very sensitive exercise and cannot be based on an ideal case assumption. In Chapter 3, we discover that analytical solution requires an accurate phase measurement as input and because phase measurement is unreliable data with lots of errors, we have to work with magnitude of Γ_{in} only.

Chapter 3

3 Analytical Solution

In Chapter 3, a thorough mathematical analysis has been developed to integrate the Q factors of each component into a sample pi-circuit. In such setup, the system is expected to calculate the antenna impedance, Z_L using a pre-set initial capacitance values of pi-circuit. Then, using the computed Z_L we can use the conjugate matching method to find the 3 DTC values. Thus, in the analysis of Chapter 3, we assume that Z_L is already found by accurate calibration and Z_1, Z_2 and Z_3 are the unknowns.

The pi-tuner is practically turned into L-network depending on the load impedance condition - z_L either inside or outside the 1+jx circle. Then, three capacitor values are computed by conjugate matching between Z_o and Z_{in} (including antenna impedance Z_L). To make the mathematics easier, the left branch of the pi-tuner is effectively excluded from Z_{in} and instead added to Z_o side as shown in Figure 3-1. [13]

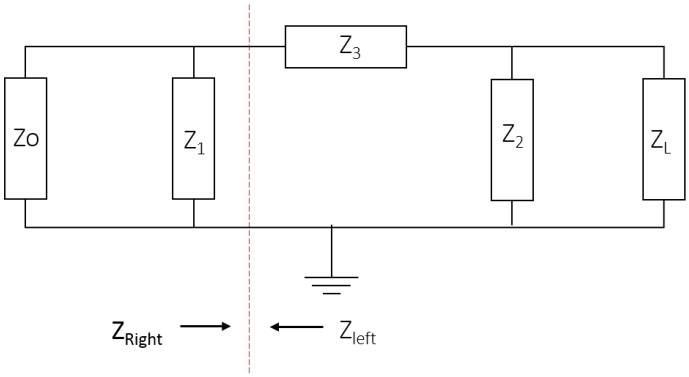

FIGURE 3-1: TURNING PI NETWORK INTO L NETWORK

As a result, Γ_{in} is not always zero because altering the defining boundary of Z_{in} no longer meets the condition, $Z_{in} = Z_o = 50\Omega$. Instead, the analytical solution for capacitance is obtained by *minimizing* Γ_{in} by $\frac{\partial \Gamma_{in}}{\partial C_n} = 0$ for all capacitors (n=1,2,3). [13] Minimizing Γ_{in} to be the closest to the ideal matched condition of 0 (or 50Ω) or VSWR to 1 is desirable in impedance matching.

$$VSWR_{in} = \frac{1 + |\Gamma_{in}|}{1 - |\Gamma_{in}|} \qquad (21)$$

While the analytical solution for capacitance guarantees maximum power transfer from the source to the altered Z_{in} in theory, the effect of impedance mismatch between the pi-tuner and antenna ($\Gamma_L = \Gamma_{out}^*$) is still questionable. (But this is not related to that the analytical solution does not provide a non-zero Γ_{in}.)

After forcing impedance match, $\Gamma_{in} = \Gamma_S^*$, G_T would effectively provide the appropriate measure of power gain by the load from the power delivered to the system with the insight of pi-tuner's internal loss S_{21}. Thus, maximizing G_T is used as an alternate technique for analytical solution and is done by evaluating the relative transducer gain. [13]

$$\Delta G_T = \frac{|S_{21}|^2}{|1 - S_{22}\Gamma_L|^2} \tag{22}$$

G_T is used to compare several solutions after $\Gamma_{in} = \Gamma_S^*$. [1]

$$G_T = \frac{P_L}{P_{for\ network}} = \frac{|S_{21}|^2(1 - |\Gamma_S|^2)(1 - |\Gamma_L|^2)}{|1 - \Gamma_S\Gamma_{in}|^2\ \ |1 - S_{22}\Gamma_L|^2} \tag{23}$$

The matched impedance of the matching network with the load seen at the port of the transmission line eliminates the reflected signal flowing back. This indicates that the maximum power is delivered to the load and the Total Radiated Power (TRP) is maximized. Also, signal-to-noise ratio of the system is improved for other components in the RF chain such as the antenna, low-noise amplifier and power amplifier, yielding an increased Total Isotropic Sensitivity (TIS). PA efficiency will increase and saves current. [18]

As common practice, PAs are protected from the reflected signal from the antenna by the use of isolator that reroute the reflected signal into a load to be dissipated by heat. With impedance tuning network, this isolator can be removed to save cost and space in device. [18]

Conjugate matching is a valid approach to guarantee maximum power transfer from the source. The radio system impedance is 50Ω and $Z_G(= Z_o)$ is ideally real. Then, $\Gamma_{\text{in}} = 0$ is achieved at the center of the Smith Chart by various impedance matching techniques. [1]

3.1 Solution without Q Factor

As an example, for the case when the boundary is drawn as shown in Figure 3-1 in pi-network, conjugate match can be calculated starting with two expressions for the impedance Z of the left and right side.

This section closely follows the work provided in [13].

$$Z_{left} = Z_o||Z_1 \tag{24}$$

$$Z_{right} = (Z_L||Z_2) + Z_3 \tag{25}$$

$$Z_{left} = Z_o||Z_1 = \frac{1}{\frac{1}{(Ro + I{\cdot}Xo)} + \frac{1}{(R1 + I{\cdot}X1)}} \tag{26}$$

And the real and imaginary part of (26) can be defined as

$$f(R_o, X_o, R_1, X_1) = \frac{\frac{Ro}{Ro^2 + Xo^2} + \frac{R1}{R1^2 + X1^2}}{\left(\frac{Ro}{Ro^2 + Xo^2} + \frac{R1}{R1^2 + X1^2}\right)^2 + \left(-\frac{Xo}{Ro^2 + Xo^2} - \frac{X1}{R1^2 + X1^2}\right)^2} \tag{27}$$

$$g(R_o, X_o, R_1, X_1) = -\frac{\left(-\frac{Xo}{Ro^2 + Xo^2} - \frac{X1}{R1^2 + X1^2}\right)}{\left(\frac{Ro}{Ro^2 + Xo^2} + \frac{R1}{R1^2 + X1^2}\right)^2 + \left(-\frac{Xo}{Ro^2 + Xo^2} - \frac{X1}{R1^2 + X1^2}\right)^2} \tag{28}$$

$$so\ that, \qquad Z_{left} = Z_o||Z_1 = f(R_o, X_o, R_1, X_1) + j \cdot g(R_o, X_o, R_1, X_1) \tag{29}$$

Similarly,

$$Z_{right} = Z_L||Z_2 + Z_3 = f'(R_L, X_L, R_2, X_2) + j \cdot g'(R_L, X_L, R_2, X_2) + Z_3 \tag{30}$$

Note that $Z_o||Z_1$ and $Z_L||Z_2$ expressions have symmetrical relationship; Their real and imaginary terms are both functions of R and X of two branches in parallel.

The Z_3 branch alone is purely reactive, contributing to *only the imaginary term, g',* of Z_{right}.

Now we can summarize Z_{left} and Z_{right} as :

$$Z_{left} = Re\{Z_{left}\} + Im\{Z_{left}\} \tag{31}$$

$$Re\{Z_{left}\} = f(R_o, X_o, R_1, X_1) \tag{32}$$

$$Im\{Z_{left}\} = g(R_o, X_o, R_1, X_1) \tag{33}$$

$$Z_{right} = Re\{Z_{right}\} + Im\{Z_{right}\} \tag{34}$$

$$Re\{Z_{right}\} = f(R_L, X_L, R_2, X_2) \tag{35}$$

$$Im\{Z_{right}\} = g(R_L, X_L, R_2, X_2) + Im\{Z_3\} \tag{36}$$

When $R_L > R_o$, Z_1 branch will be turned off and by setting $Re\{Z_{left}\} = Re\{Z_{right}\}$, the only unknown parameter is Z_2 (= R_2 + jX_2). After calculating Z_2, $Im\{Z_{left}\} = -Im\{Z_{right}\}$ will help solve for Z_3. Similarly, when $R_L < R_o$, Z_2 branch will be turned off, Z_1 branch will be calculated first for resistance match and then Z_3 from opposite sign reactance match. [13]

In any case, if the solution for a capacitor is not suitable for the given range of the capacitor already mounted on design, the value could be fixed to either minimum or maximum and the remaining capacitors can be computed to satisfy (37). [13]

$$\frac{d|\Gamma_{in}|}{dC_x} = 0 \ (for\ X = 1, 2\ or\ 3) \tag{37}$$

$$\mathrm{Z}_{in} = \frac{\left(\frac{Z_L Z_2}{Z_L + Z_2} + Z_3\right) Z_1}{\left(\frac{Z_L Z_2}{Z_L + Z_2} + Z_3\right) + Z_1} \tag{38}$$

$$\Gamma_{in} = \frac{Z_{in} - Z_o}{Z_{in} + Z_o} \tag{39}$$

If the solutions from such analysis discussed so far is not suitable for the range of the tunable capacitor, the algorithm can alter the sequence of capacitors to tune – for example, starting with Z_3 and tuning Z_1 and Z_2 to different combinations of maximum and minimum stage and choosing the case with the best transducer gain. [13]

Anyhow, this analytical solution discussed in [13] takes *ideal* components and does not count for the Q factor. Also, often, these three branches could be a network of L and C themselves. Thirdly, once the ideal components are practically represented in the circuit, with equivalent resistance from qualify factor Q, the solutions of capacitance rising from $Re\{Z_{left}\} = Re\{Z_{right}\}$ and $Im\{Z_{left}\} = -Im\{Z_{right}\}$ will no longer provide a way to solve for C2 and C3 one after the other by substitution. The main reason is that Z3 now contributes to $Re\{Z_{right}\}$ as well.

3.2 Solution with Q-Factor

In this section, we build on the work from [13] to find a more general approach to solve pi-network that counts for quality factors of all components as well, both L and C, in a Pi-network shown in Figure 3-2.

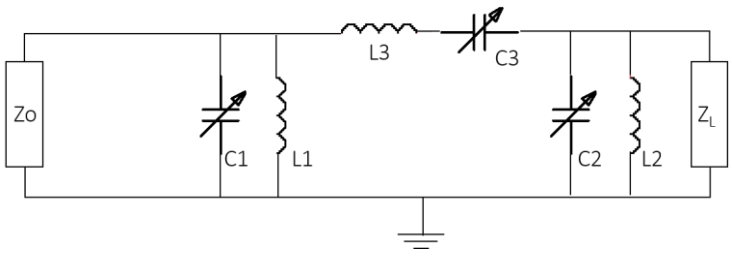

FIGURE 3-2: PI-TUNER CIRCUIT.

Impedance of a practical capacitor with the Q factor provided by the manufacturer can be expressed with a parallel resistance. Similarly, a practical inductor can be expressed with a series resistance [13].

$$Z_L = 2\pi f L\left(\frac{1}{Q_L} + j\right) \tag{40}$$

$$Y_C = 2\pi f C\left(\frac{1}{Q_c} + j\right) \tag{41}$$

After taking Q factors of all components into account, Figure 3-2 becomes much more complex for analytical solution, as shown in Figure 3-3.

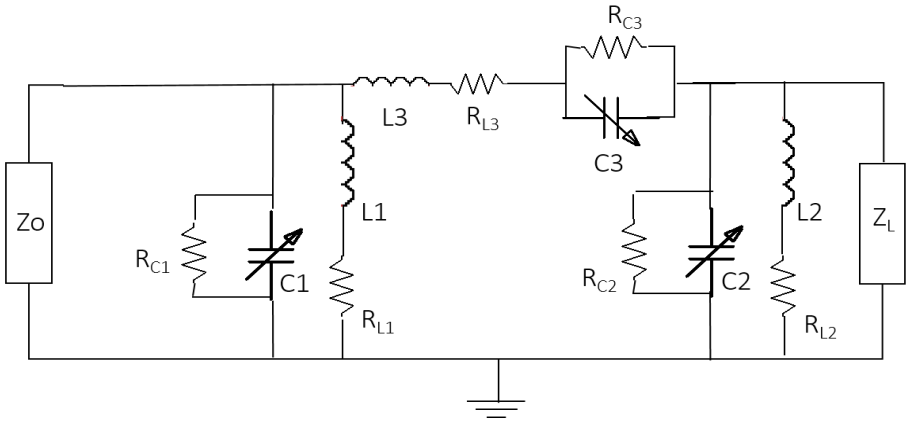

FIGURE 3-3: PI-TUNER CIRCUIT WITH Q-FACTOR AND EQUIVALENT RESISTANCE FOR COMPONENTS.

No matter how complex each branch in pi-tuner is, we can express it in terms of impedance and admittance as Appendix A shows for Figure 3-3.

Therefore, the main challenge of this derivation solely lies in computing the derivative of Zin, or $\frac{d|\Gamma_{in}|}{dC_x} = 0$, in terms of each capacitor abiding to equations (37) and (39). Employing equation-solving libraries from software tools is not desirable since the resulting equations would be too complex and impractical for microcontroller implementation.

Note how each branch can be simplified as shown in Figure 3-4, with admittance Y and impedance Z. We have defined Z_{Left}, Z_{right} and Z_{middle} slightly differently from the previous section.

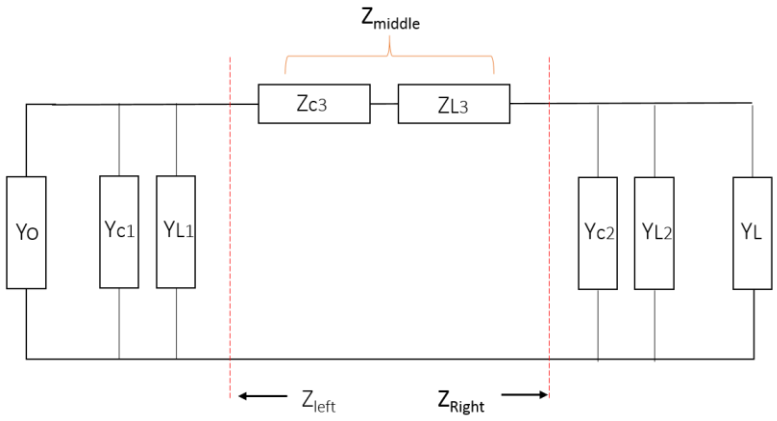

FIGURE 3-4: SIMPLIFIED PI-TUNER CIRCUIT

First, Z_{left} can be expressed as real and imaginary parts,

$$Z_{left} = \frac{1}{Y_o + Y_{C1} + Y_{L1}} = \frac{1}{(G_o + jB_o) + (G_{C1} + jB_{C1}) + (G_{L1} + jB_{L1})} \tag{42}$$

$$Z_{left} = \frac{G_o + G_{C1} + G_{L1}}{(G_o + G_{C1} + G_{L1})^2 + (B_o + B_{C1} + B_{L1})^2} - j\frac{B_o + B_{C1} + B_{L1}}{(G_o + G_{C1} + G_{L1})^2 + (B_o + B_{C1} + B_{L1})^2} \tag{43}$$

Similarly, Z_{right} can also be expressed as real and imaginary parts as shown in (45).

$$Z_{right} = \frac{1}{Y_L + Y_{C2} + Y_{L2}} = \frac{1}{(G_L + jB_L) + (G_{C2} + jB_{C2}) + (G_{L2} + jB_{L2})} \tag{44}$$

$$Z_{right} = \frac{G_L + G_{C2} + G_{L2}}{(G_L + G_{C2} + G_{L2})^2 + (B_L + B_{C2} + B_{L2})^2} - j\frac{B_L + B_{C2} + B_{L2}}{(G_L + G_{C2} + G_{L2})^2 + (B_L + B_{C2} + B_{L2})^2} \tag{45}$$

And Z_{middle} is ,

$$Z_{middle} = (R_{C3} + R_{L3}) + j(X_{C3} + X_{L3}) \tag{46}$$

As we draw the boundary for intermediate real match, at the boundary for Z_{left} in Figure 3-4, we expect the real and imaginary parts to match between the left and the right side such that,

$$Re\{Z_{left}\} = Re\{Z_{right}\} + Re\{Z_{middle}\} \tag{47}$$

$$-Im\{Z_{left}\} = Im\{Z_{right}\} + Im\{Z_{middle}\} \tag{48}$$

Then, we get two equations, (49) and (50), for real and imaginary parts.

$$\frac{G_o + G_{C1} + G_{L1}}{(G_o + G_{C1} + G_{L1})^2 + (B_o + B_{C1} + B_{L1})^2} = (R_{C3} + R_{L3}) + \frac{G_L + G_{C2} + G_{L2}}{(G_L + G_{C2} + G_{L2})^2 + (B_L + B_{C2} + B_{L2})^2} \tag{49}$$

$$\frac{B_o + B_{C1} + B_{L1}}{(G_o + G_{C1} + G_{L1})^2 + (B_o + B_{C1} + B_{L1})^2} = (X_{C3} + X_{L3}) - \frac{B_L + B_{C2} + B_{L2}}{(G_L + G_{C2} + G_{L2})^2 + (B_L + B_{C2} + B_{L2})^2} \tag{50}$$

3.2.1 Left branch turned off

When the left branch is turned off (C_1=C_{1min}), terms associated with C_1 become known in (49) and when we compute all the known variables and let it be $T1_{Re}$ (51), the resistance match equation becomes an equation of two unknown variables C_2 and C_3 (52) .

$$T1_{Re} = \frac{G_o + G_{C1} + G_{L1}}{(G_o + G_{C1} + G_{L1})^2 + (B_o + B_{C1} + B_{L1})^2} - R_{L3} \tag{51}$$

$$T1_{Re} = \boldsymbol{R_{C3}} + \frac{G_L + \boldsymbol{G_{C2}} + G_{L2}}{(G_L + \boldsymbol{G_{C2}} + G_{L2})^2 + (B_L + \boldsymbol{B_{C2}} + B_{L2})^2} \tag{52}$$

If we let,

$$G_{C2} = \frac{2\pi f C_2}{Q_{C2}(f)} = K_{C2}(f) \cdot C_2 \tag{53}$$

$$B_{C2} = 2\pi f C_2 = K_{C2}(f) \cdot Q_{C2}(f) \cdot C_2 \tag{54}$$

$$G_L' = G_L + G_{L2} \tag{55}$$

$$B_L' = B_L + B_{L2} \tag{56}$$

we can obtain a more thorough expression for (52):

$$T1_{Re} = \frac{K_{C3}C_3}{(K_{C3}Q_{C3}C_3)^2 + (K_{C3}C_3)^2} + \frac{K_{C2}C_2 + G_L'}{(K_{C2}C_2 + G_L')^2 + (K_{C2}C_2Q_{C2} + B_L')^2} \tag{57}$$

Similarly, the conjugate imaginary part match equation (50) becomes an equation of two unknown variables C_2 and C_3 as well, and also get an expression for $T1_{Im}$ (59).

$$T1_{Im} = \frac{B_o + B_{C1} + B_{L1}}{(G_o + G_{C1} + G_{L1})^2 + (B_o + B_{C1} + B_{L1})^2} - X_{L3} \tag{58}$$

$$T1_{Im} = X_{C3} - \frac{B_L + B_{C2} + B_{L2}}{(G_L + G_{C2} + G_{L2})^2 + (B_L + B_{C2} + B_{L2})^2} \tag{59}$$

Using (59), we get a more thorough expression for (59) for the unknown variables:

$$T1_{Im} = -\frac{K_{C3} Q_{C3} C_3}{(K_{C3} Q_{C3} C_3)^2 + (K_{C3} C_3)^2} - \frac{K_{C2} C_2 Q_2 + B_L{}'}{(K_{C2} C_2 + G_L{}')^2 + (K_{C2} C_2 Q_{C2} + B_L{}')^2} \tag{60}$$

Equation (57) and (60) are difficult to solve for C2 and C3. *Iteration method* is suitable for such case. We define $T1_{Re}$ again, with C_3 (known) and $T1_{Im}$ with C_2 (known) when substitutions are made.

$$T1'_{Re} = T1_{Re} - \frac{K_{C3} C_3}{(K_{C3} Q_{C3} C_3)^2 + (K_{C3} C_3)^2} \tag{61}$$

$(T1'_{Re}: T1_{Re}\ updated\ with\ C_3)$

$$T1'_{Re} = -\frac{K_{C2} C_2 + G_L{}'}{(K_{C2} C_2 + G'_L)^2 + (K_{C2} C_2 Q_{C2} + B'_L)^2} \tag{62}$$

Solving for C_2 gives :

$$C_2 = -\frac{1}{2} \cdot \frac{1}{T1'_{Re}\left(Q_{C2}{}^2 + 1\right) K_{C2}} \left(2B'_L Q_{C2} T1'_{Re} + 2G'_L T1'_{Re} \pm \sqrt{T1'_{Re}{}^2 (-4G'^2_L Q_{C2}{}^2 + 8B'_L G'_L Q_{C2} - 4B'^2_L) + Q_{C2} T1'_{Re} (4G'_L Q_{C2} - 4B'_L) + 1} - 1 \right) \tag{63}$$

After finding C_2, we can update $T1'_{Im}$ and find C_3,

$$T1'_{Im} = T1_{Im} + \frac{K_{C2} C_2 Q_2 + B_L{}'}{(K_{C2} C_2 + G_L{}')^2 + (K_{C2} C_2 Q_{C2} + B_L{}')^2} \tag{64}$$

$$T1'_{Im} = -\frac{K_{C3} Q_{C3} C_3}{(K_{C3} Q_{C3} C_3)^2 + (K_{C3} C_3)^2} \tag{65}$$

$$C_3 = -\frac{1}{K_{C3} T1'_{Im} (Q_{C3}^2 + 1)} \tag{66}$$

This solution for C_3 will be substituted to equation for C2 after updating $T1_{Re}$.

After 2 iterations, starting with C_3=0, analytical solutions for C_2 and C_3 accounting for their manufacturer quality factor can be found.

3.2.2 Right branch turned off

When the right branch is turned off ($C_2 = C_{2min}$), the procedure is similar. Using (49), terms associated with C_2 become known (67) and the resistance match equation becomes an equation of two unknown variables C_1 and C_3 (68).

$$T2_{Re} = R_{L3} + \frac{G_L + G_{C2} + G_{L2}}{(G_L + G_{C2} + G_{L2})^2 + (B_L + B_{C2} + B_{L2})^2} \tag{67}$$

$$T2_{Re} = -R_{C3} + \frac{G_o + G_{C1} + G_{L1}}{(G_o + G_{C1} + G_{L1})^2 + (B_o + B_{C1} + B_{L1})^2} \tag{68}$$

By letting $G_o' = G_o + G_{L1}$ and $B_o' = B_o + B_{L1}$,

$$T2_{Re} = -\frac{K_{C3}C_3}{(K_{C3}Q_{C3}C_3)^2 + (K_{C3}C_3)^2} + \frac{K_{C2}C_1 + G_o'}{(K_{C1}C_1 + G_o')^2 + (K_{C1}C_1Q_{C1} + B_o')^2} \tag{69}$$

And the updated term with C_3 would be,

$$T2'_{Re} = T2_{Re} + \frac{K_{C3}C_3}{(K_{C3}Q_{C3}C_3)^2 + (K_{C3}C_3)^2} \tag{70}$$

$$T2'_{Re} = \frac{K_{C2}C_1 + G_o'}{(K_{C1}C_1 + G_o')^2 + (K_{C1}C_1Q_{C1} + B_o')^2} \tag{71}$$

Now solving for C_1 gives:

$$C_1 = -\frac{1}{2} \cdot \frac{1}{T2'_{Re}\left(Q_{C2}{}^2 + 1\right)K_{C2}} \tag{72}$$

$$\left(2B_o'Q_{C2}T2'_{Re} + 2G_o'T2'_{Re}\right.$$

$$\left. \pm \sqrt{T2'_{Re}{}^2(-4G_o'{}^2Q_{C2}{}^2 + 8B_o'G_o'Q_{C2} - 4B_o'{}^2) + Q_{C2}T2'_{Re}(4G_o'Q_{C2} - 4B_o') + 1} - 1\right)$$

After finding C_1, we can update $T2'_{Im}$ and find C_3. Once we know that,

$$T2_{Im} = \frac{B_L + B_{C2} + B_{L2}}{(G_L + G_{C2} + G_{L2})^2 + (B_L + B_{C2} + B_{L2})^2} - X_{L3} \tag{73}$$

We can get ,

$$T2_{Im} = X_{C3} - \frac{B_o + B_{C1} + B_{L1}}{(G_o + G_{C1} + G_{L1})^2 + (B_o + B_{C1} + B_{L1})^2} \tag{74}$$

$$T2_{Im} = -\frac{K_{C3}Q_{C3}C_3}{(K_{C3}Q_{C3}C_3)^2 + (K_{C3}C_3)^2} - \frac{K_{C1}C_1Q_1 + B_o'}{(K_{C1}C_1 + G_o')^2 + (K_{C1}C_1Q_{C1} + B_o')^2} \tag{75}$$

Let

$$T2'_{Im} = T2_{Im} + \frac{K_{C1}C_1Q_1 + B_o{}'}{(K_{C1}C_1 + G_o{}')^2 + (K_{C1}C_1Q_{C1} + B_o{}')^2} \tag{76}$$

And using iteration with (69) and (75),

$$T2'_{Im} = -\frac{K_{C3}Q_{C3}C_3}{(K_{C3}Q_{C3}C_3)^2 + (K_{C3}C_3)^2} \tag{77}$$

$$C_3 = -\frac{1}{K_{C3}T2'_{Im}(Q_{C3}^2 + 1)} \tag{78}$$

For cases when the solutions for capacitance are not within the physical tuning range of the chosen capacitor, the algorithm gets more complex. The solution will be forced to be the minimum of the tuning range if it is below or maximum of the tuning range if it is over the range. Then, the last remaining capacitor has to be computed to yield as small VSWR as possible by means of computing equation.

$$\frac{d|\Gamma_{in}|}{dC_x} = 0 \ (for\ X = 1, 2\ or\ 3) \tag{79}$$

The computation of capacitance for minimum VSWR is very complicated starting with Zin.

$$Z_{in} = \frac{1}{\dfrac{1}{Z_{L3} + Z_{C3} + \dfrac{1}{Y_{C2} + Y_{L2} + Y_L}} + Y_{C1} + Y_{L1}} \tag{80}$$

$$Z_{in} = \frac{(Y_{C2} + Y_{L2} + Y_L)(Z_{L3} + Z_{C3}) + 1}{(Y_{C2} + Y_{L2} + Y_L) + ((Y_{C2} + Y_{L2} + Y_L)(Z_{L3} + Z_{C3}) + 1)(Y_{C1} + Y_{L1})} \tag{81}$$

$$\Gamma_{in} = \frac{\dfrac{(Y_{C2} + Y_{L2} + Y_L)(Z_{L3} + Z_{C3}) + 1}{(Y_{C2} + Y_{L2} + Y_L) + ((Y_{C2} + Y_{L2} + Y_L)(Z_{L3} + Z_{C3}) + 1)(Y_{C1} + Y_{L1})} - Z_o}{\dfrac{(Y_{C2} + Y_{L2} + Y_L)(Z_{L3} + Z_{C3}) + 1}{(Y_{C2} + Y_{L2} + Y_L) + ((Y_{C2} + Y_{L2} + Y_L)(Z_{L3} + Z_{C3}) + 1)(Y_{C1} + Y_{L1})} + Z_o} \tag{82}$$

We note that Γ_{in} is a fraction of complex numbers (83) and VSWR involves the absolute value of Γ_{in}. If we set x as one of the capacitors, C1, C2 or C3, while the other two are known, the complex number fraction, Γ_{in} can be expressed as (83) while A, B, C and D are real, first-order functions of x.

$$\Gamma_{in} = \frac{A(x) + jB(x)}{C(x) + jD(x)} \tag{83}$$

Then, the magnitude of Γ_{in} becomes

$$|\Gamma_{in}| = \sqrt{\frac{A(x)^2 + B(x)^2}{C(x)^2 + D(x)^2}} \tag{84}$$

And taking the derivative of absolute value and letting it equal to zero as (37) will result in:

$$[A(x)A'(x) + B(x)B'(x)][C^2(x) + D^2(x)] - [C(x)C'(x) + D(x)D'(x)][A^2(x) + B^2(x)] = 0 \quad (85)$$

After all, it is possible to derive the equation for C_1, C_2 and C_3 with (85). However, after computing it in terms of parameters found in Appendix A, the equation is practically too large for embedded programming.

3.3 Open-loop Procedure

Once the magnitude and phase of Γ_{in} are found and the configuration in Figure 2-1 are entirely calibrated, we can start with an open-loop configuration. A sample procedure of finding the solution analytically in [14] can be simplified as :

1) Determine [S] matrix of pi-tuner ***with*** the initial setting for the reactive components.
2) The system is characterized with 1) and once we measure the phase and magnitude of Γ_{in}, we can theoretically calculate the impedance of the load, Z_{Load}, with calibration parameters in calculation.
3) Once Z_{Load} is determined, we can use the analytical method in Section 3 to find C_1, C_2 and C_3 values.
4) Optionally, the system can lead to a closed-loop configuration by algorithm, once the analytical solution needs further fine tuning. [18]

3.3.1 Difficulties of Open-Loop System for Analytical Solution

Open-loop and closed-loop control are often combined to take the advantage of both systems. [18][19] However, with the following difficulties, in this thesis, we strictly focus on closed-loop, a measurement-based system for the following reasons.

- Phase measurement of Γ_{in} from AD8302 was not consistent and showed large dependence on the reflected signal strength, transmitted signal strength, and also the impedance of the antenna. While Z_L is the unknown parameter, it is not possible to calibrate for magnitude and phase measurement for all different values of Z_L.
- The PCB layout of the Pi-tuner has its EM effect. It is possible to use software tools to carry out EM simulation and de-embed the board. A successful simulation would still add few degrees of error for the phase.
- The phase reading from the phase detector (AD8302) was not consistent. We see in others work [18] that phase measurement is too erroneous and unreliable.
- The set up in Figure 3-1 was hard to calibrate. Each sweep or measurement after system boot-up in application setting will have unreliable variation.

- The DTCs' capacitance does not have linear correspondence to the voltage level applied. Also, the capacitance versus voltage graph varies along with other factors such as Q factor, temperature and frequency. Therefore, even after computing the capacitance of the components, it is highly inaccurate to use the best-fit polynomial equation for all cases.

Each problem has a proposed solution to reduce the degree of error. However, the uncertainty is still large and is hard to troubleshoot once these factors collide in calibrating the system.

Importantly, even with low VSWR solution, when the Z_{in} is low and reflected signal is high, the matching performance of analytical solution would be extremely poor and result is unpredictable. Therefore, it is unavoidable to implement the closed loop condition with a searching algorithm on the microprocessor.

3.4 Closed Loop System

For Chapter 4 and 5, the set up introduced in Figure 3-1 will no longer employ two AD8302 for phase measurement since phase measurement is not reliable. The algorithms discussed in this thesis will solely rely on magnitude measurement only, with one AD8302. The new setup is now much simpler as shown in Figure 3-5.

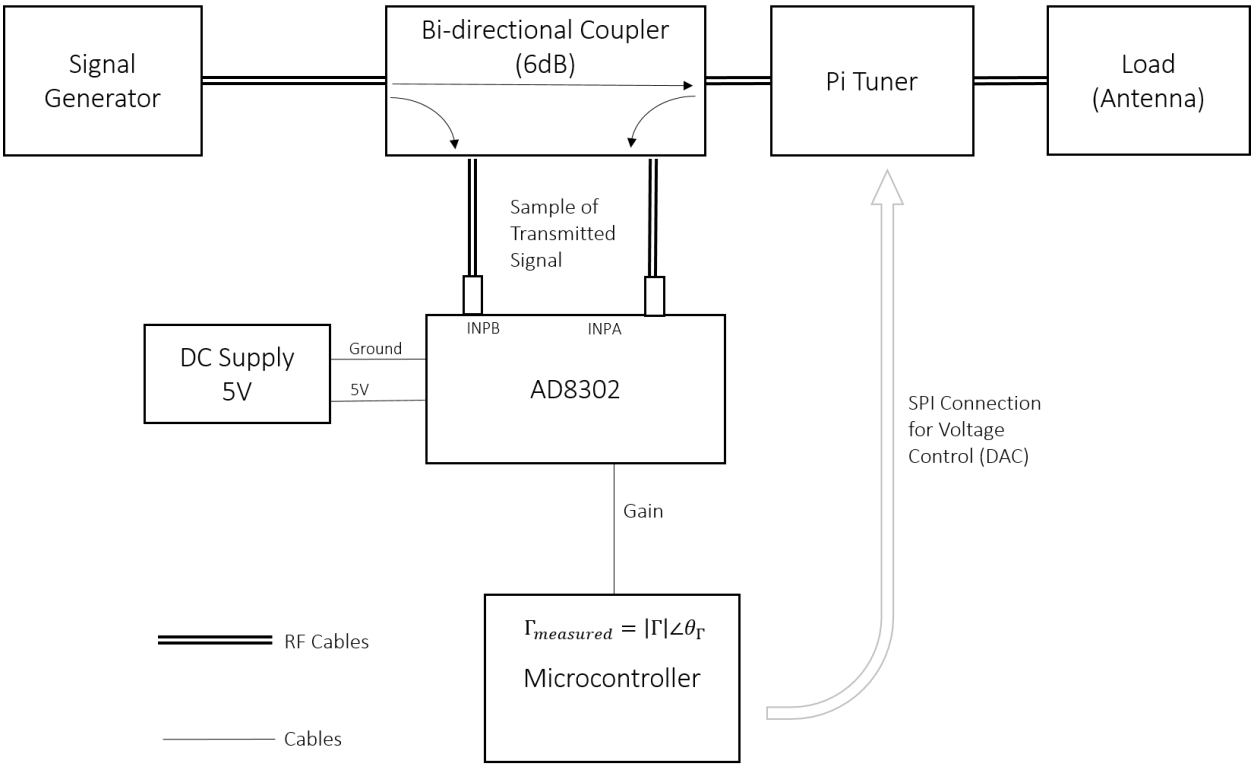

FIGURE 3-5: IMPEDANCE MATCHING SYSTEM WITH ONE AD8302.

Chapter 4

4 Hill Climbing Algorithm

4.1 Theory

Hill climbing is a well-known and popular choice for optimization among many mathematical applications. From an initial point on a convex or concave surface defined by $f(\boldsymbol{X})$, where $\boldsymbol{X}$ is a vector, hill-climbing will take an increment of the position, evaluate $f(\boldsymbol{X})$, and iterate the process until the change in $f(\boldsymbol{X})$, improves.

In Pi-tuning network, there are three capacitors and the Γ_{in} (which we will call the measured S11) will change as we tune the DTCs. This can be applied on a 3-dimensional space, choosing x, y and z axis to represent each of the capacitors and the space to be the gradient field of Γ_{in}.

Hill climbing solution is known to converge on a local solution (maximum or minimum), rather than the global solution. [20] Also, the solution will vary depending on the choice of the increment size. There are various ways to implement hill-climbing search for our application.

4.2 Implementation

For hill climbing algorithm, it will start at an arbitrary point and iterate the search until it reaches a pre-set condition – for example, that the Γ_{in} is either below -10 dB or stop iteration when it does not improve further after certain number of trials. The flow chart of the algorithm is shown in Figure 4-1. In this algorithm, we have chosen 8 candidates that are equally spaced out around the point in consideration.

Hill climbing algorithm has several variables:

- Increment size
- Number of candidates
- Number of search trials
- Matching requirement (ex: -10dB)
- Settling requirement

Appendix B presents the raw output of microprocessor from our setup. B.1-B.4 were all implemented with the same increment size of 1 V applied to the DTCs and to start from different initial values of DTCs.

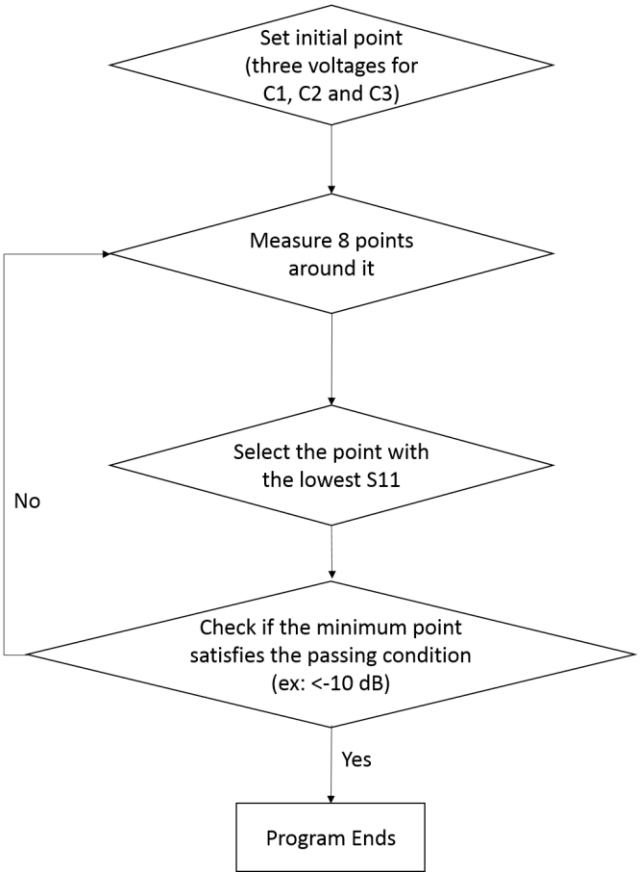

FIGURE 4-1: HILL CLIMBING ALGORITHM FLOW CHART.

In Appendix B.1, when the initial point is from (C1, C2, C3) = (3.95V, 3.95V, 3.95V), after 16 iterations, we obtained the solution that passes the matching requirement, Γ_{in} < -10dB. B.2 shows an unstable convergence after starting from point (4.89V, 4.89V, 4.89V). B.3 and B.4 show rather quick convergence.

In hill climbing algorithm, we see that when the solution is hidden very finely in the gradient and the increment size is too large, the local minimum solution is not the best solution.

Chapter 5

5 Grid Search Algorithm

Same as hill climbing algorithm, grid search algorithm relies on empirical data of $|\Gamma_{in}|$ measurement form AD8302. Disregarding the phase of Γ_{in}, the solution will only focus on matching for the best $VSWR_{in}(=\frac{1+|\Gamma_{in}|}{1-|\Gamma_{in}|})$.

Instead of starting from an initial point and exploring the surroundings on the plane, grid search algorithm will scan the entire gradient. The challenge lies in optimizing the accuracy against the number of data points measured. More data points will result in an unacceptable level of speed and less data points could simply be insufficient to understand the whole gradient.

In this thesis, we are using the pi-network circuit which entails three digitally tunable capacitors, therefore allowing three degrees of freedom. Same as Chapter 4, we can represent the data collection of reflection coefficient as a gradient in 3D space, with each of the capacitors represented by the axis (x, y, z).

The axis represents the voltage level applied to the capacitor. It is important to note that the voltage applied to the capacitor does not have a linear correspondence to the capacitance. Here, the algorithm will only refer to the voltage level it feeds to the capacitors as input variable. In most of the data in this section, the voltage applied to the DTCs are represented by the DAC values sent via SPI connection from the microprocessor. The DAC values and the voltages have a linear relationship and can be used interchangeably. (Lower DAC value means lower voltage.)

5.1 Algorithm Design

5.1.1 Understanding Measurement Data

The 3D data representation with three axis for each capacitance is hard to visualize or represent on paper. Hence, to represent the gradient, we draw the Γ_{in} as a plane with DAC C1 and C2 only at only three different levels of DAC C3, as shown in Figure 5-1. The x and y axis both represent the voltage level or DAC value sent to two capacitors by SPI, C1 and C2, with very fine steps. Here, we have fixed the third capacitor at three distinct levels and collected the data points for three sets.

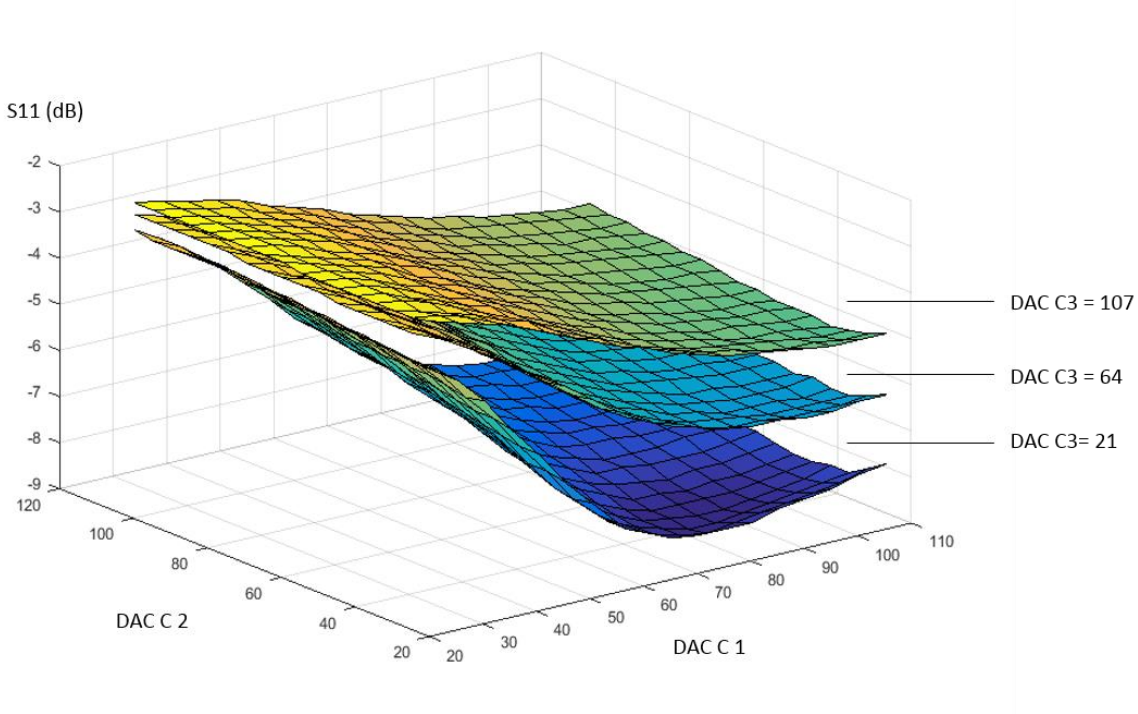

FIGURE 5-1: A SAMPLE PLANE REPRESENTATION OF Γ_{in} DATA POINTS

By observing the curvature of these planes, if we picture x-, y- and -z- axis as DAC C1, C2 and C3, we can predict that Γ_{in} measurement along any line parallel to axis will be a curve – a polynomial less than 3rd degree. In other words, if we fix the two capacitors and collect the data points by tuning only one capacitor, the resulting Γ_{in} graph will have one local maximum and/or one local minimum at most. More accurately, the graph, over the range of the tuned capacitor, would be a portion or subset of a full-period sinusoidal wave form.

We can also verify this trend on the Smith Chart as we fix two capacitors and tune one capacitor. Then, the longest possible path of S11 draws a path less than a full circle. Hence, the graph will have one local minimum and/or one local maximum. In most cases, we see that it draws a half circle, resulting in a stretched convex or concave curve.

As an example, in order to characterize the S11 curve, we take three parallel lines to DAC C2 axis at maximum C3 value and measure S11 by tuning C2 only as shown in Figure 5-2.

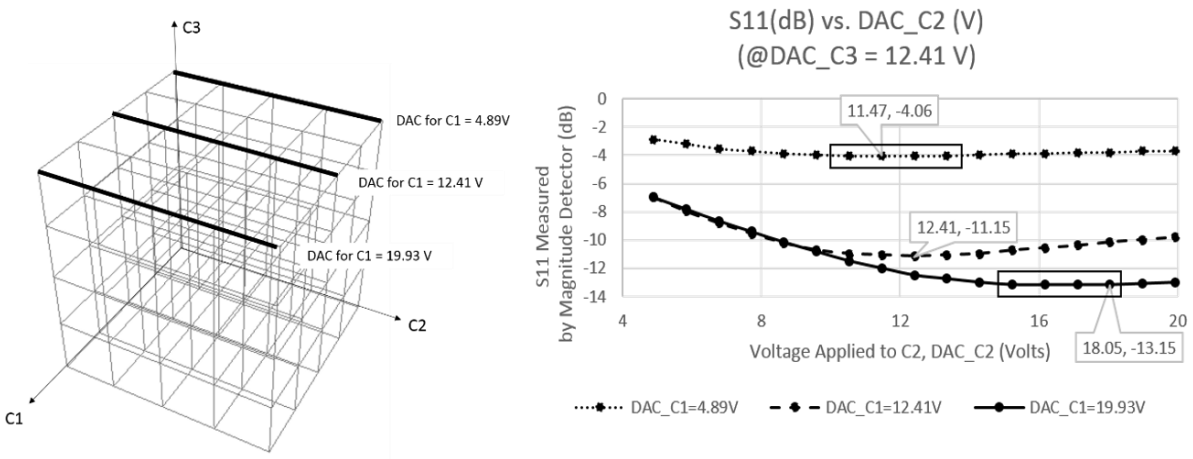

FIGURE 5-2: SAMPLE CHARACTERIZATION OF Γ_{in} CURVE FOR DC_C3 = 12.41 V BY TUNING DAC C2.

5.1.2 Iterative Interpolation

A polynomial can be expressed as $y(x) = a_n x^n + a_{n-1} x^{n-1} + \cdots + a_1 x + a_0$. Many methods of **polynomial interpolation** involve unique formulas and in most cases, more data points help to obtain more accurate curve fitting.

As mentioned before, tuning just one capacitor makes a curve or a polynomial less than 3rd-degree - that is, a cubic function, $y = ax^3 + bx^2 + cx + d$. It is commonly known that we need information of the roots to solve a cubic function but in our application, we cannot use this approach because we cannot locate the roots without fine scanning, which is undesirable.

For three tunable capacitors in pi-network, setting N=3 (number of data points) will result in 27=3x3x3 measurements. Similarly, setting N=4 will result in 64. In such case, if we make the search process iterative by selecting a region to zoom-in further, it will be much more effective than a non-iterative process that scans all data points across the gradient. In other words, taking more points for initial gradient investigation (higher N) yields the best *initial* resolution but the speed will suffer (high Ntotal) due to wasting time mostly on measuring wrong areas.

For a quick comparison of the number of points per one iteration's grid scan, let:

- I: number of iterations
- N: number of measurements per line [unit: points]
- N_total : total number of measurements for 3D region [unit: points]
- X: ratio of the length of initial line after reduction [unit: ratio]

- R: ratio of initial volume after reduction [unit: ratio]
- K: number of steps for voltage level

And

$$N_{total} = N^3 \times I \quad (86)$$

$$X_{smaller} = \frac{1}{(N-1)^I}, \quad X_{larger} = \frac{1}{[2(N-1)]^I} \quad (87)$$

$$R = X^3 = \frac{1}{(N-1)^{3\times I}} \quad (88)$$

Comparison for varying N is shown in Table 5-1.

TABLE 5-1: N-POINT GRID SEARCH TOTAL NUMBER OF DATA POINTS COMPARISON

Number of iterations (I)	3-point grid search (N=3) (N_{total}, X, R)	4-point grid search (N=4) (N_{total}, X, R)	5-point grid search (N=5) (N_{total}, X, R)	6-point grid search (N=6) (N_{total}, X, R)
1	$N_{total} = 27\ points$ $X = 1/2$ $R = 1/8$	$64\ points$ $1/3$ $1/27$	$125\ points$ $1/4$ $1/64$	6*6*6=216 points 1/5 1/125
2	$N_{total} = 54\ points$ $X = 1/4$ $R = 1/64$	64 * 2 = 128 points 1/9 1/729	125*2=250 points 1/16 1/4096	216*2=432 points 1/25 1/15625
3	$N_{total} = 81\ points$ $X = 1/8$ $R = 1/512$	64 * 3 = 192 points 1/27 1/19683	125*3=375 points 1/64 1/262144	~~216*2=1296~~ 1/125 (resolution reached maximum)
4	$N_{total} = 108\ points$ $X = 1/16$ $R = 1/4096$	64 * 4 = 256 points 1/81 1/531441	~~125*4=500~~ 1/256 (resolution reached maximum)	
5	$N_{total} = 135\ points$ $X = 1/32$ $R = 1/32768$	~~64 * 5 = 320~~ 1/243 (resolution reached maximum)		
6	$N_{total} = 162\ points$ $X = 1/64$ $R = 1/262144$			
7	~~$N_{total} = 189\ points$~~ $X = 1/128$ (resolution reached maximum)			

For the case when K=81 steps, iteration stops when X no longer meets $K = 81 > \frac{1}{X}$, which is the limit of fine tuning for our DTCs. In fact, when N=4, at fourth iteration I=4, the region is reduced to resolution R=1/531441 by having 256 measurements. When N=6, the resolution is only at R=1/125 by having 216 measurements in the first iteration.

Here, reducing the number of points is the key challenge. In the Hill Climbing algorithm, each iteration requires 8 measurements and 80 measurements mean 10 iterations. Though Hill Climbing search does not guarantee convergence into global minimum, requiring few hundred measurements is a significant disadvantage for Grid Search algorithm.

In Figure 5-1, we have used more than 8000 points of data to draw three planes. In order to obtain a sharp solution, the grid step has to be fine, requiring an intensively long process of scanning, but most of the measurements away from our solution will be useless. In fact, if the algorithm intelligently zooms closer to the solution without fully scanning the entire grid, it will be much more efficient, which points to the iterative interpolation method with N=3.

5.1.3 Selecting Zoom-in Regions

Once we force the grid to be initialized by N=3, 27 points as shown in Figure 5-3, it requires an algorithm to define the boundary of reduced region for zoom-in.

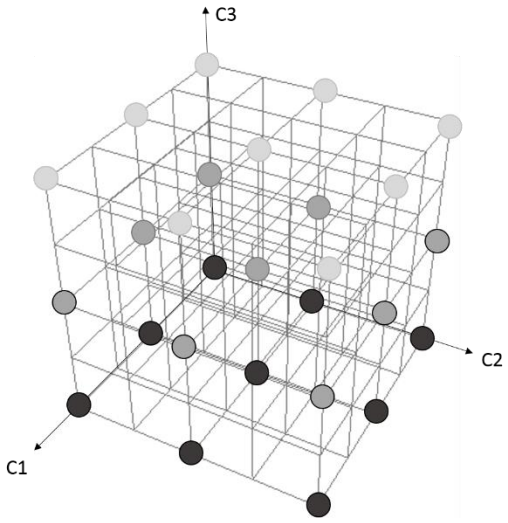

FIGURE 5-3: N=3, LOCATION OF 27 DATA POINTS FOR INITIAL SCANNING OF S11 GRID

After we scan 27 points, we can identify the point with the minimum Γ_{in} and define the region for the next iteration around it. However, there is a problem when we do this with just 3x3x3 points. Consider the Γ_{in} curve in Figure 5-2. If the minimum of three points is on either of the ends - 0 or 1 of the length - the region of search along the line could effectively be [0 ~ 0.25] or [0.75 ~ 1] of the range. But if the minimum among the three points is the middle point, setting the region as [0.25 ~ 0.75] is risky.

This is shown in Appendix C, where we characterize an antenna entirely for all directions of the gradient. We see that the Γ_{in} curve sometimes when the curvature is flat, the minimum could exist outside the boundary of [0.25, 0.75] such as somewhere around 0.2 of the length.

In that case, the algorithm will miss the global minimum at 0.2 and continue its iteration into [0.25, 0.75]. The algorithm is likely to converge at the edge of the region, 0.25, but it is still far away from the global minimum. Such scenario happens when the gradient has flat curvature because the antenna has poor impedance match overall in the first stage of iteration. It is worth addressing this issue.

One way to cover the risk of leaking global minimum is to do two parallel searches with separate regions from two minimum points, which we will call 'branches'. Two regions will go through iteration separately and each branch will converge to a solution. However, this is not enough to prevent leaking the solution.

Another effort to reduce the risk is to examine the line containing the minimum point by 5-point measurement as shown in Figure 5-4. Given that the curve is less than 3rd order polynomial, 5 point is sufficient enough to guarantee that the selected region around the point with the lowest value will contain the hidden minimum along the line.

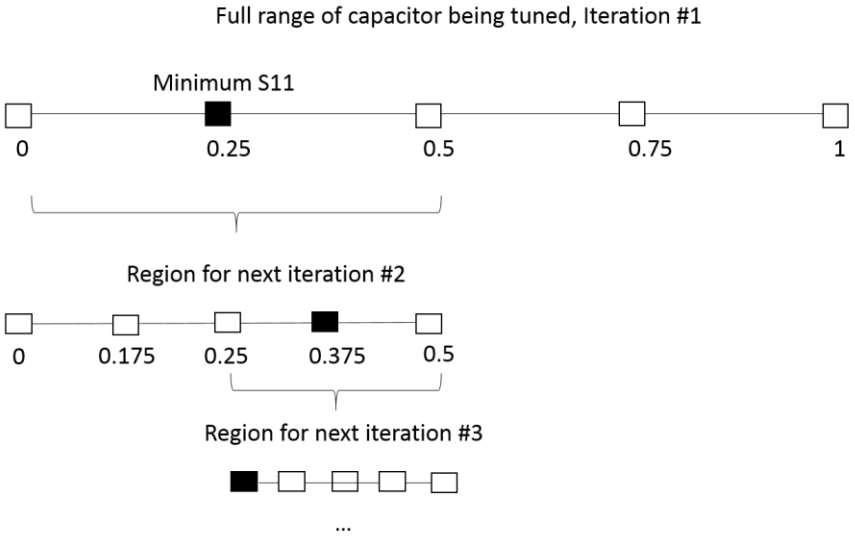

FIGURE 5-4: ALGORITHM FOR SELECTING ITERATION REGION WITH 5-POINT MEASUREMENT

5-point measurement will definitely provide more intuition and coverage for the solution. However, it is obviously undesirable to apply this to all three axis, because one iteration will become 125 points. Instead, we have to select only one plane as a perspective angle and apply 5-point measurement along one direction only.

For this matter, we can choose to use any of the 6 plane orientations shown in Figure 5-5. Each plane can be looked at by two directions and there are 9 segments or branches for each direction.

When we select the point with the minimum Γ_{in} among the 27 points, the segment containing the minimum point will be the branch for the first iteration. The second branch will be selected with the second minimum Γ_{in} outside the first segment.

Once the two segments or branches are selected out of 9, we will apply 5 point measurement along the line and select the region as shown in Figure 5-4 along the line, which will become the length of the rectangular box region for the next iteration. For the cross section of the box, we just define it to be around the point as discussed before. Once the rectangular box has been defined, the algorithm will do a 3x3x3 scan again within the box and so on. Note that from the second iteration might not yield a cubic box.

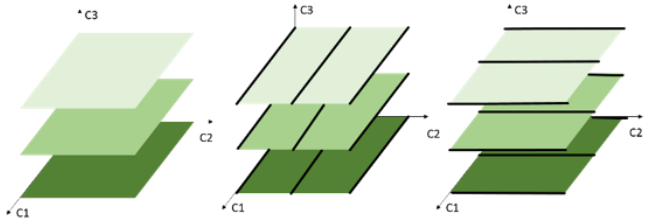

(a) XY-plane

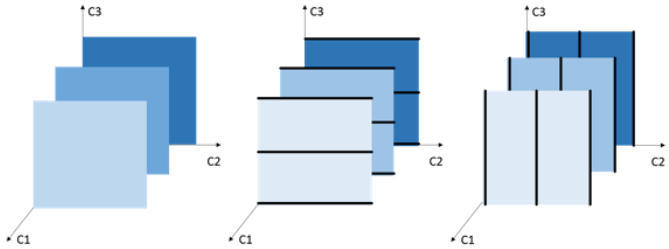

(b) YZ-plane

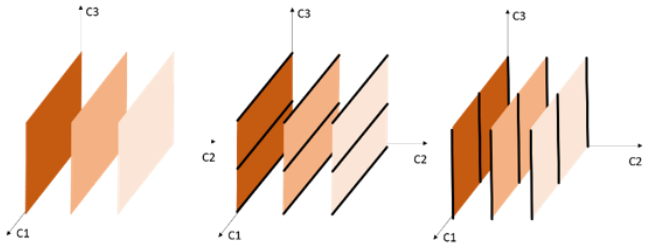

(b) XZ-plane

FIGURE 5-5: PLANE REPRESENTATIONS AFTER N=3, 27-POINT GRID SEARCH

5.1.4 Branches

Table 5-2 calculates the total number of measurements when we employ both methods discussed in previous section to ensure that we do not miss the global point.

Let, N_{total} be the number of measurements taken and X_{small} and X_{large} be the smallest and largest possible region along one axis. When the box is formed around a segment that is in the middle of the initial box, we use X_{large} and when the box is on the edge of the initial box, we use X_{small}.

$$N_{total} = 3^3 \times I + 5 \times I \tag{89}$$

$$X_{small} = \left(\frac{1}{4}\right)^I, \quad X_{large} = \left(\frac{1}{2}\right)^I \tag{90}$$

Table 5-2: Number of iterations calculated with additional 5-point fine tuning

Number of iterations (I)	Branch 1	Branch 2
1	$N_{total} = 32\ points$ $X_{small} = 1/4$	
2	$N_{total} = 64\ points$ $X = 1/16$	$N_{total} = 64\ points$ $X = 1/16$
3	$N_{total} = 96\ points$ $X = 1/64$	$N_{total} = 96\ points$ $X = 1/64$
Total measurement = 32 ×5 + 5 = 165 points		

Here, we see that total measurement of 165 points are needed to search into two branches. If we can clarify that only one branch is sufficient, the required measurement will be reduced to about half, 32×3=96 points.

As shown in Table 5-3, in most of the cases, the first branch would yield the global minimum. However, in some cases, the second branch would include the global minimum such as Case 3. In some cases, the third branch could perform better than the second branch such as Case 4, but it would not be better than first branch. Sometimes, the first and second branch have the same measurement and the outcome is unpredictable.

While the third branch is proven to be unnecessary to be considered, the second branch remains of question. Since the gap of the final solutions of the first and second branch are small even when the second branch has a better solution (less than 1 dB), we may only keep one branch as it would reduce the time by almost

half. If the application can allow a long time for matching, including parallel iteration for two branches is strongly suggested.

Table 5-3: Top three branches and global minimum

Case #	Top 3 Minimum from Initial Grid Sweep of 27 points	Top 3 Regions After convergence from each branch	Global Minimum found without algorithm
1	(21, 106, 106) : -10.73 (dB) (63, 106, 63) : -6.73 (dB) (63, 63, 106) : -5.64 (dB)	(28, 106, 106) : -14.90 (dB) (36, 106, 84) : -10.40 (dB) (31, 84, 106) : -10.31 (dB)	(31, 106, 106): -15.10(dB)
2	(63, 21, 106) : -12.32 (dB) (106, 63, 106) : -10.31 (dB) (106, 106, 106) : -8.98 (dB)	(89, 36, 106) : -13.40 (dB) (95, 42, 106) : -11.73 (dB) (84, 52, 89) : -10.31 (dB)	(91, 31, 106): -13.20 (dB)
3	(63, 63, 106) : -19.49 (dB) (63, 106, 106) : -18.66 (dB) (106, 106, 63) : -17.07 (dB)	(68, 84, 106) : -23.66 (dB) (73, 106, 106) : -24.33 (dB) (84, 103, 84) : -18.24 (dB)	(76, 106, 106): -25.00 (dB)
4	(63, 106, 106) : -24.24 (dB) (63, 106, 63) : -15.82 (dB) (63, 63, 106) : -13.48 (dB)	(57, 100, 106) : -27.16 (dB) (62, 106, 84) : -21.91 (dB) (52, 84, 103) : -23.58 (dB)	(56, 106, 101): -27.66 (dB)
5	(63, 21, 106) : -6.89 (dB) (106, 63, 106) : -6.89 (dB) (106, 106, 63) : -6.56 (dB)	(84, 36, 100) : -6.98 (dB) (84, 52, 89) : -6.31 (dB) (94, 89, 52) : -4.64 (dB)	(86, 36, 101): -8.56 (dB)

5.2 Characterization

According to Figure 5-5, we have tried to characterize a full dataset with three perspective angles – xy plane, yz plane and xz plane. In Appendix C, we have shown how Figure 5-6 (a) data was obtained as an example.

For each plane with three layers, we have marked the segments with the lower Γ_{in} measurements in two directions. After compiling it all in three directions, we have overlapping regions agreed by three perspective angles as shown in (d) in Figure 5-6.

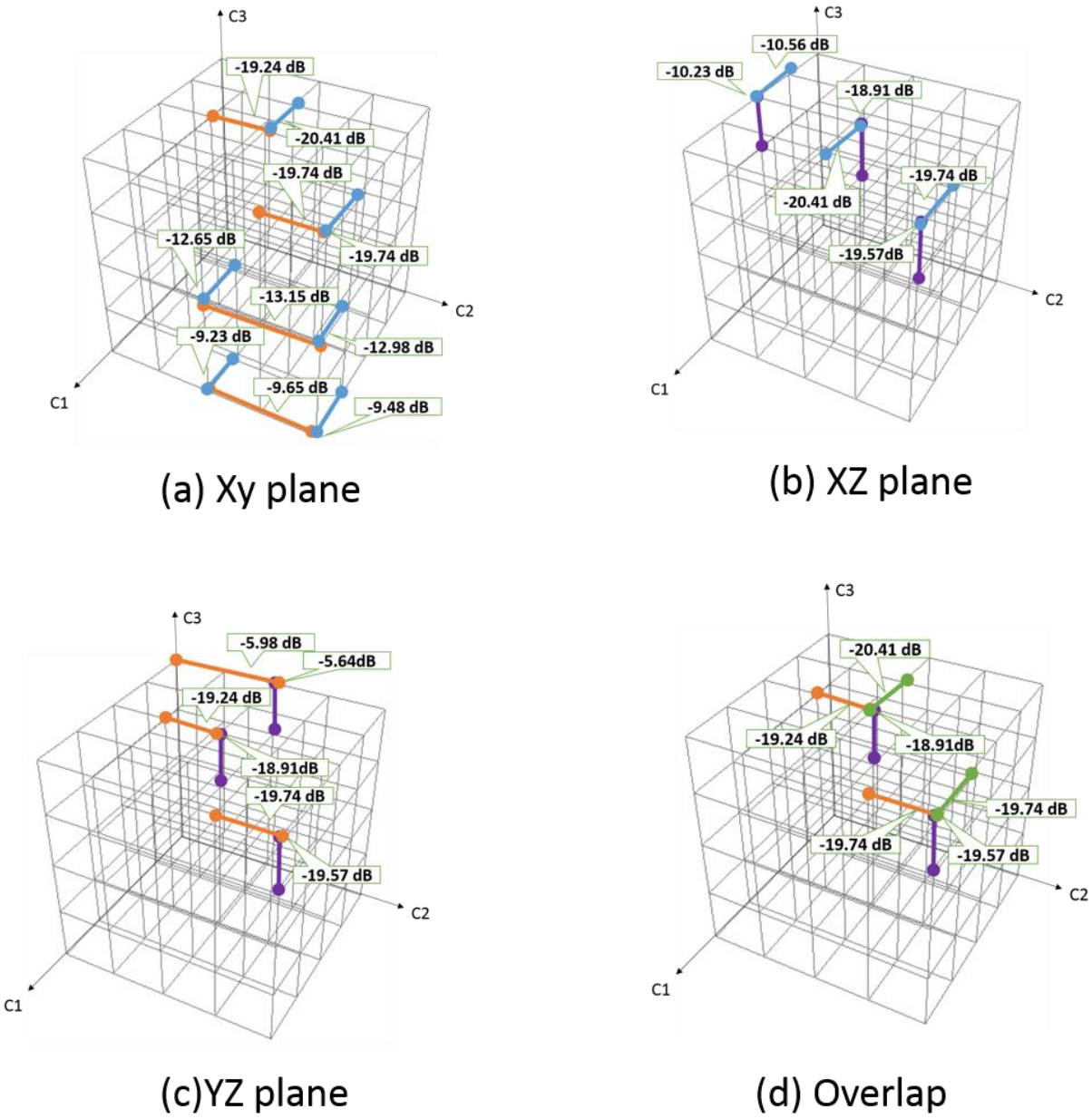

FIGURE 5-6: DATA CHARACTERIZATION AT DIFFERENT PLANES

This is a meaningful result because it allows us to only search for data at one perspective angle – such as xy plane – and by intelligently selecting the search region around the data point, we can inclusively keep the global point that remains throughout the iteration and eventually converge to the solution.

In other words, the method of selecting the region around the minimum Γ_{in} measurement point, seen at one side of the cube, guarantees the same solution from other sides of the cube.

5.3 Result

In this section, we see two scenarios of data that results from the grid search algorithm – two frequencies 2.4 GHz and 2.45GHz for an antenna operating in 2.4 GHz frequency. It is to visually present how each iteration reduces the region and merge into global solution.

We used,

- two branches of iteration in the algorithm for each case.
- the 5-point measurement is along C1 axis.
- Each case is represented with its Γ_{in} gradient by full scanning with fine tuning to verify the result from the algorithm.

The grid search algorithm result is for the specific frequency of the signal. The device would have to run the algorithm again when it is operating on a different frequency.

5.2.2 Result at 2.4 GHz

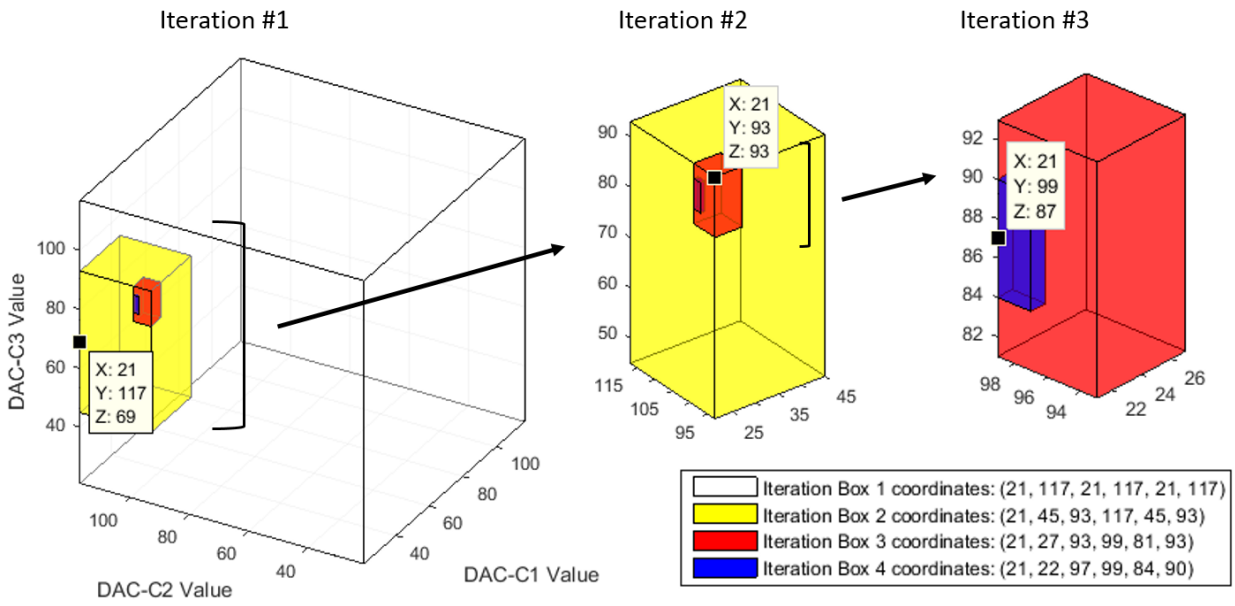

FIGURE 5-7: GRID SEARCH ALGORITHM FOR ANTENNA A – 2.4GHZ – BRANCH 1

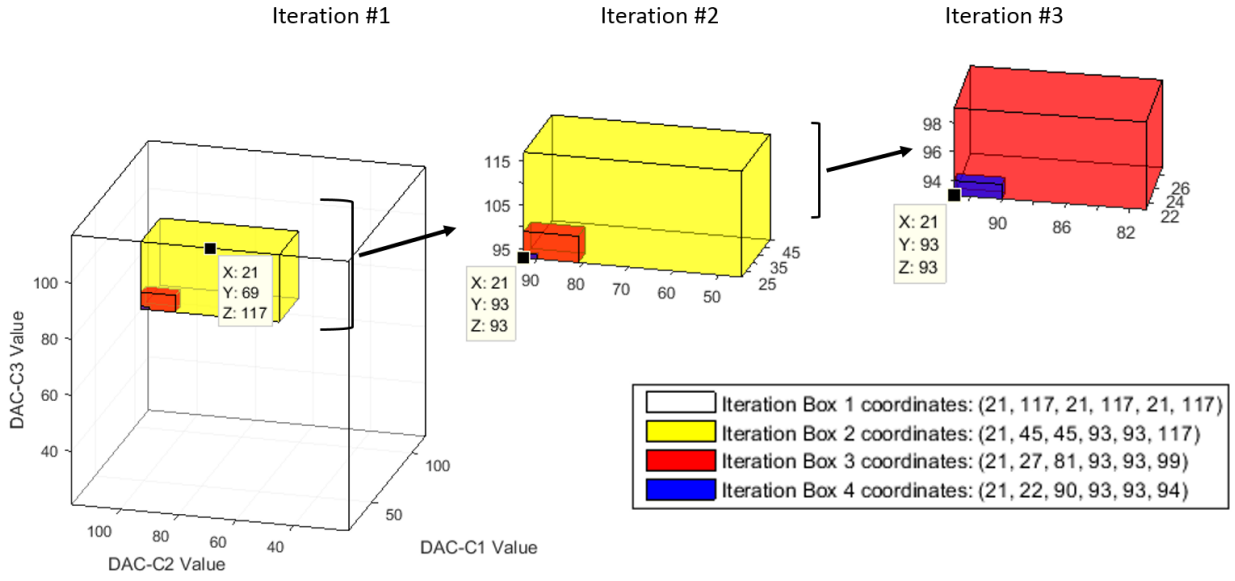

FIGURE 5-8: GRID SEARCH ALGORITHM FOR ANTENNA A – 2.4GHZ – BRANCH 2

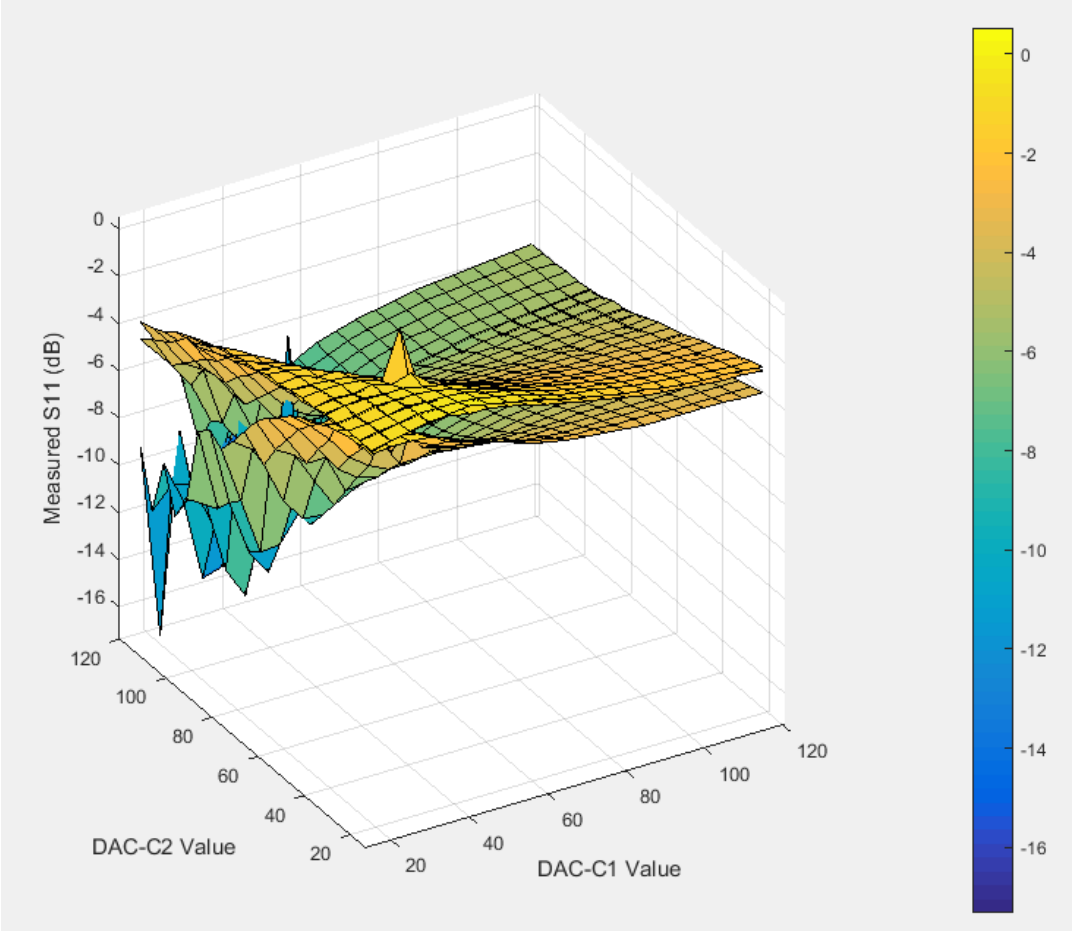

FIGURE 5-9: PLANE REPRESENTATION OF S11 MEASUREMENT BY AD8302 FOR ANTENNA A AT 2.4GHZ

We cannot see clearly in Figure 5-9, but we have (C1, C2, C3) DAC values of (22, 87, 92) to be the global minimum from the 3D space from scanning over 8000 points of data.

From Branch #1, we found (21, 99, 87) = -27.91 dB and from Branch #2, we found (21, 93, 93) = -27.75 dB to be the local minimum.

Of the two solutions, we think that solution 2 is closer to the global minimum. Therefore, Branch #2 contained the global solution and it was worthwhile to run two branches of iteration.

5.2.3 Result at 2.45 GHz

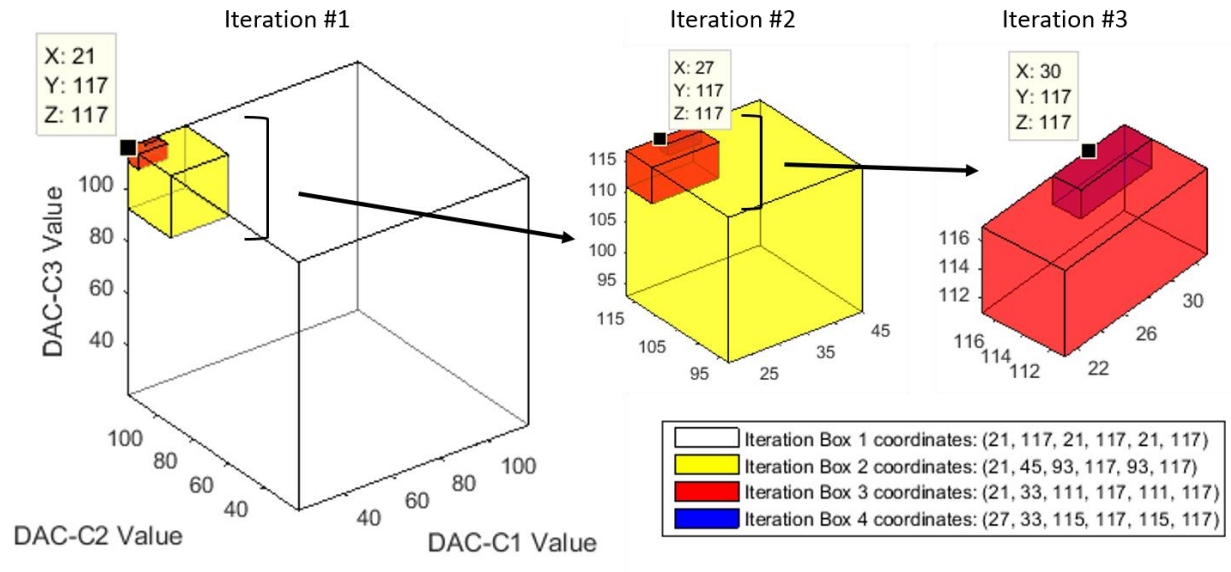

FIGURE 5-10: GRID SEARCH ALGORITHM FOR ANTENNA A – 2.45GHZ – BRANCH 1

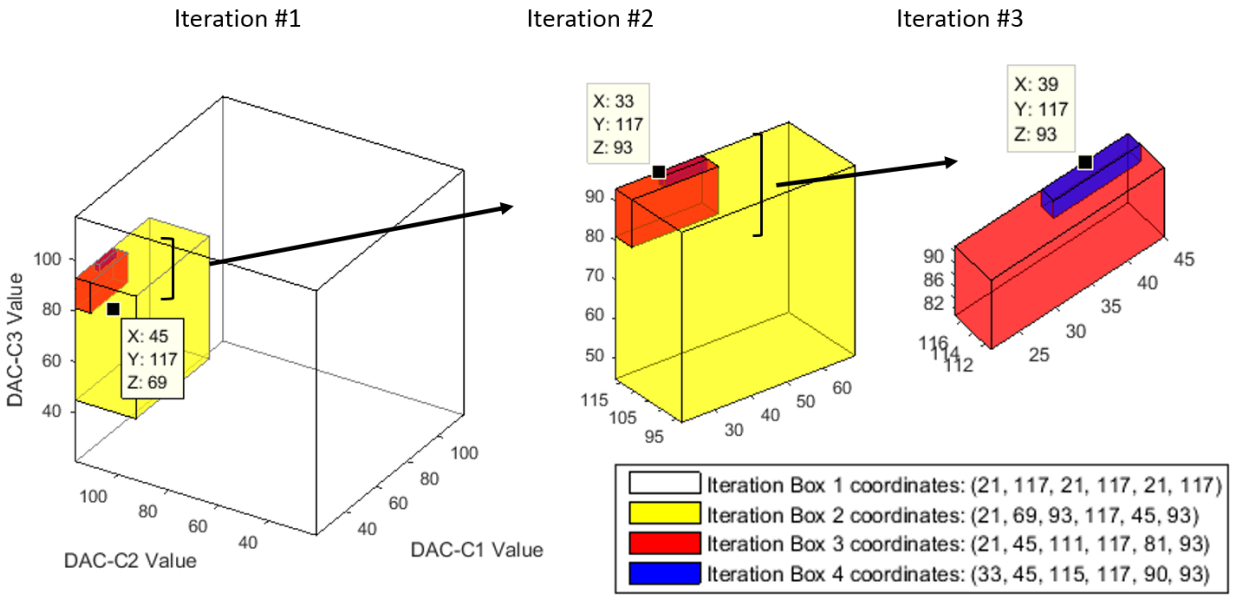

FIGURE 5-11: GRID SEARCH ALGORITHM FOR ANTENNA A – 2.45GHZ – BRANCH 2

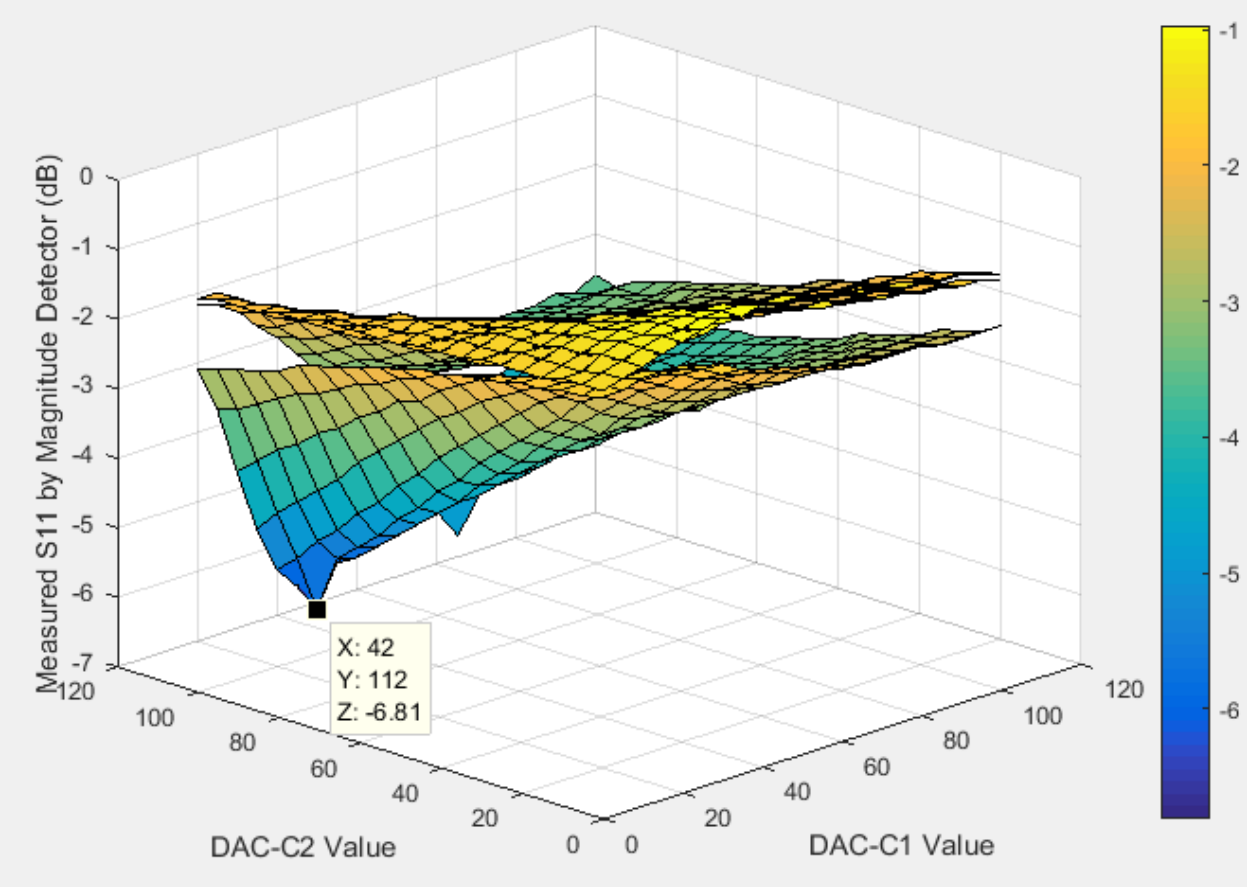

FIGURE 5-12: PLANE REPRESENTATION OF S11 MEASUREMENT BY AD8302 FOR ANTENNA A AT 2.45GHZ

We cannot see clearly in Figure 5-10, but we have (C1, C2, C3) DAC values of (22, 117, 112) to be the global minimum from the 3D space from scanning over 8000 points of data.

From Branch #1, we found (30, 117, 117) = -11.40 dB and from Branch #2, we found (39, 117, 93) = -8.06 dB to be the local minimum.

Of the two solutions, we think that solution 1 is closer to the global minimum. Therefore, Branch #1 contained the global solution and it was not worthwhile to run two branches of iteration.

5.2.4 VNA Verification

In this section, we have verified the finding from the algorithm with VNA at the RF input for f = 2.4 GHz, 2.45GHz and 2.48 GHz - that the grid search algorithm provides a better match with the chosen capacitors. We see that branch 1, most of the times, gives a better match than branch 2.

Due to the directionality of the coupler, it is difficult to sample a pure incident and reflected signal to represent the proper meaning of reflection coefficient. A separate algorithm has to be used to extract the real Γ_{in} as seen at the RF end. [21] The best method to verify the result is to run the same algorithm with the VNA's S11 measurement instead of AD8302's reading. However, this requires a very complex automation system for our setup with a special trigger connection between the VNA and the microprocessor's SPI connection. Therefore, after the matched solution has been found using the algorithm, it was verified with VNA at the RF end that the solution provides a better match compared to no matching at the particular frequency.

Figure 5-13 shows the mismatched state before running the algorithm. Figure 5-14 - Figure 5-16 show the VNA reading of real S11 at the RF end after the system has been matched with the grid search algorithm for 3 frequencies.

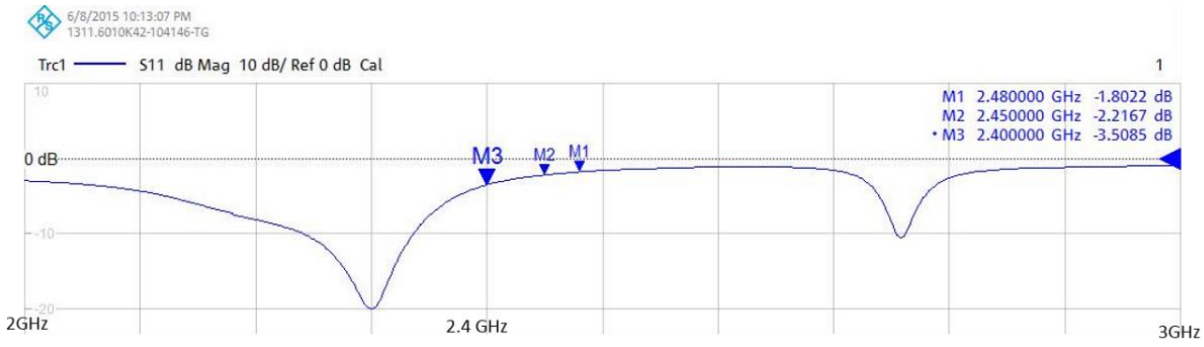

FIGURE 5-13: VNA S11 PLOT FOR ANTENNA A, UNMATCHED

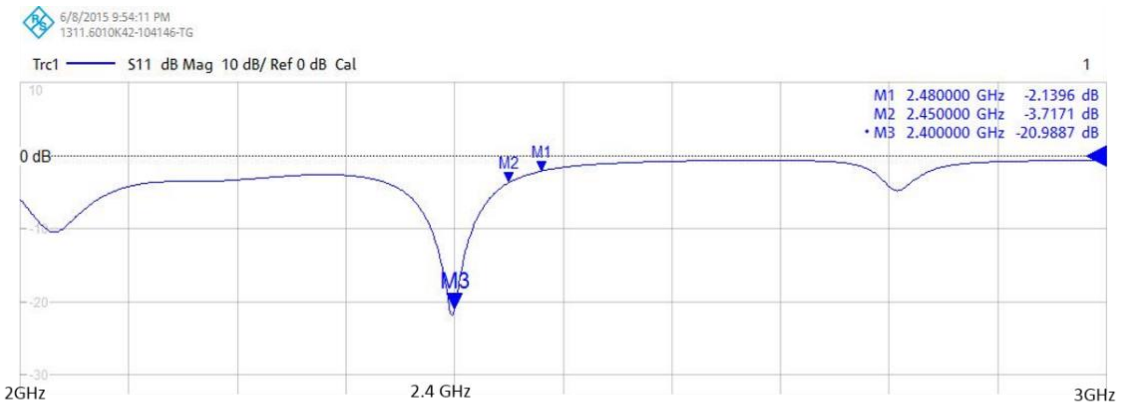

(a) Branch 1

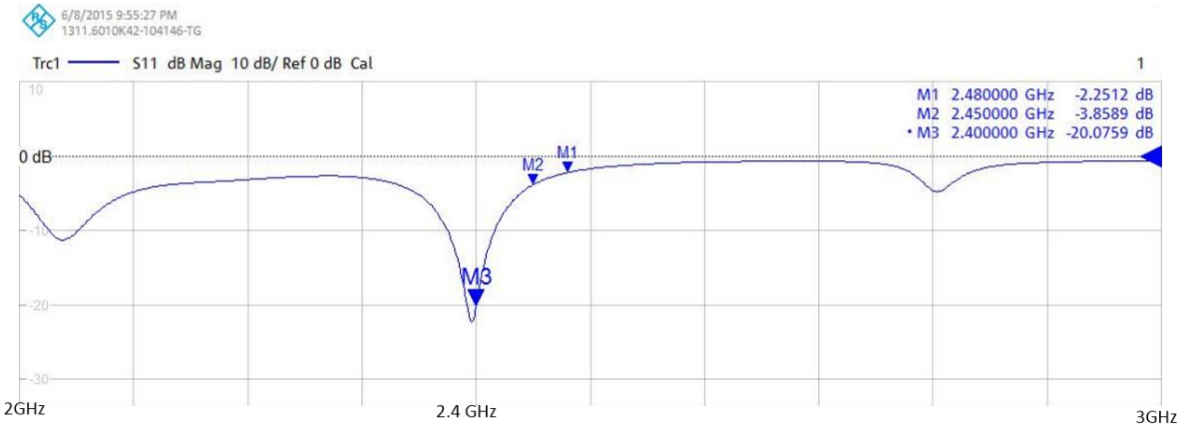

(b) Branch 2

FIGURE 5-14: VNA S11 PLOT FOR ANTENNA A, MATCHED FOR 2.4 GHZ BY GRID SEARCH ALGORITHM

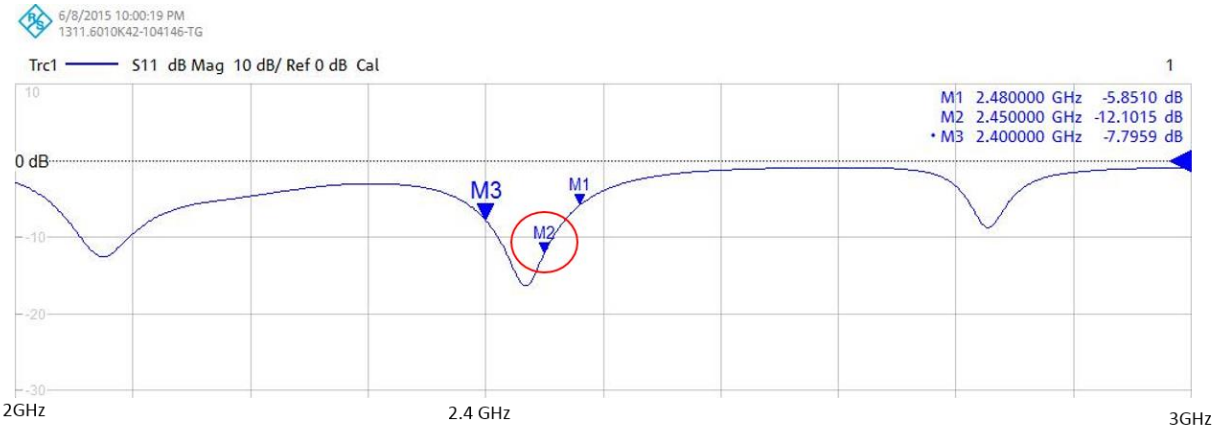

(a) Branch 1

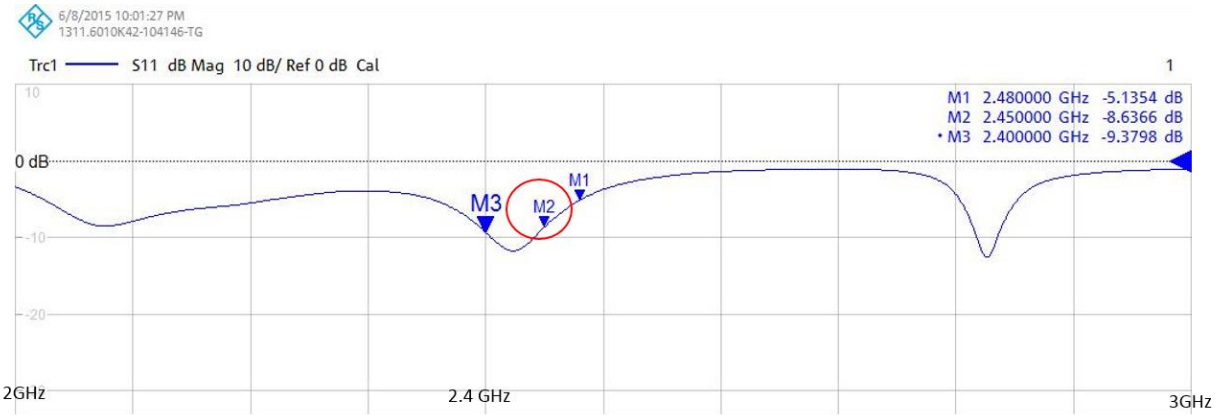

(b) Branch 2

FIGURE 5-15: VNA S11 PLOT FOR ANTENNA A, MATCHED FOR 2.45 GHZ BY GRID SEARCH ALGORITHM

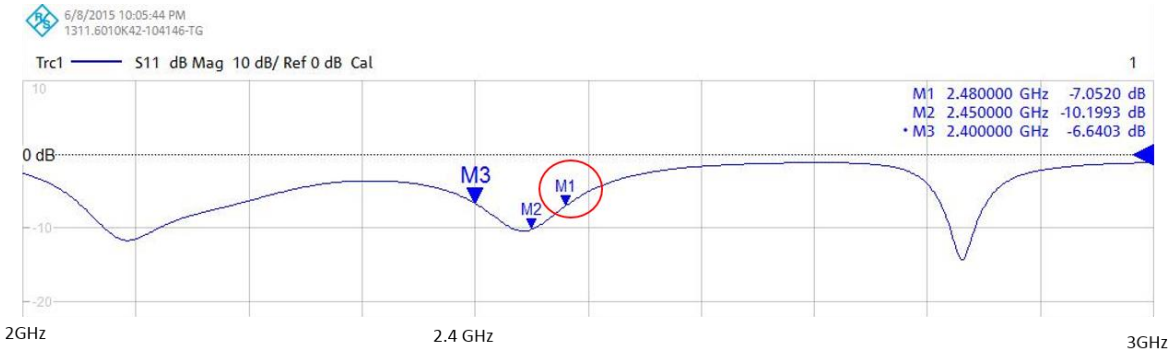

(a) Branch 1

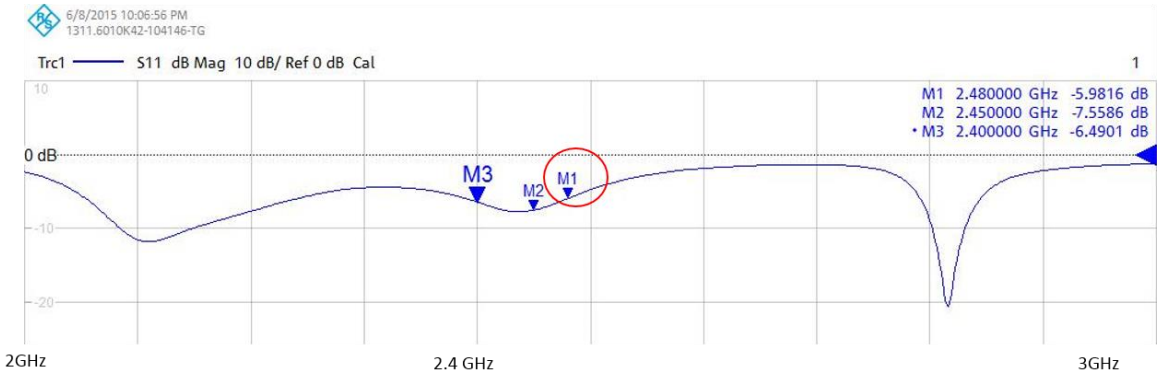

(b) Branch 2

FIGURE 5-16: VNA S11 PLOT FOR ANTENNA A, MATCHED FOR 2.48 GHZ BY GRID SEARCH ALGORITHM

Conclusions

In this thesis, we have chosen a sample pi-tuner configuration to tune the antenna impedance at the antenna input. The three DTCs in the pi-tuner allows three degrees of freedom and can be tuned via SPI connection by optimization algorithm in the microprocessor. AD8302 is a useful device to measure a parameter representative of Γ_{in} of the entire system.

In the effort to make the system an open loop configuration – a one time measurement and tuning – and make the analytical solution more practical, we have integrated the Q factor of the reactive components, both L and C, into our equations and developed the general solution for any configuration of pi-network, similar to that developed in [13] for ideal components. However, it was hard to overcome many sources of error such as: calibration of the system, limitation of phase measurement in AD8302 and the EM effect of the pi-tuner board. Even after calibrating the system, the desired voltage for calculated capacitance itself is hard to characterize and embed into algorithm.

In a closed loop configuration, hill climbing method has been practiced as a quick exercise to observe that it is not a reliable method due to its limit to converge in a local minimum.

In this thesis, the grid search algorithm is developed to guarantee a global minimum Γ_{in} solution of all possible combinations of three variables (3 DTCs). The problem is taken as a gradient 3D space defined by 3 axis representing the DTC values and take 27 (=3x3x3) points to scan and predict the location of the global point. By iteration, the defined location (or the box) will get smaller until we reach the resolution limit.

At a perspective angle, the algorithm will conduct a more detailed search (5-point measurement) for the direction only. When this method is combined with the scheme of having two branches iterating separately, it fully reduces the risk of leaking the global minimum. We have verified the answer on the full gradient.

As a real reference, VNA connected at the RF end of the system also showed the improvement of S11 after applying the algorithm and changing the state of pi-tuner accordingly. From the unmatched state of the system, all solutions for different frequency certainly showed improvement in S11 compared to the initial unmatched state.

The performance is guaranteed to yield the global minimum solution and requires only 96 measurements when it is using one branch. Compared to Hill Climbing with 8 candidates per iteration, this is only 12 iterations – where the convergence is not at the global minimum.

This is ideal for any mobile device that needs fine impedance tuning before the start of the operation, as long as there is time available for <100 measurements of S11. Exact timing requirement depends on the memory, wireless standard and microprocessor specifications.

The algorithm is simple for microcontroller programming without use of any equation-solving libraries which is a great contribute to memory. Also, since the algorithm is a 3D unconstrained optimization technique for 3 variables, it can be used in other applications such as when DTCs are used in aperture tuning. Also, there is no need to characterize or calibrate the system or generate a look-up table to use this algorithm for impedance matching.

For future work, or to improve this study, we can also incorporate the transducer gain as a second parameter to pick a better solution, apart from global minimum Γ_{in}. Maximizing (22) indicates that the maximum power is delivered to the load and the Total Radiated Power (TRP) is maximized.

$$\Delta G_T = \frac{|S_{21}|^2}{|1 - S_{22}\Gamma_L|^2}$$

In order to find the values for S_{22} and S_{21} from (22), it is wise to use the measurements from the set-up just as how Γ_{in} is measured in this thesis. However, another branch of AD8302 would need to be installed to cover two S parameters, requiring a different set-up from that used in this thesis.

Secondly, it would be ideal to optimize the solution for wider band, covering multiple frequencies with one set of solutions for DTCs. This will add frequency as a fourth variable and make the problem a 4-variable unconstrained optimization.

References

[1] D. Pozar, Microwave Engineering, Third Edition, John Wiley & Sons, Inc., New York, 2005.

[2] Elshurafa, A.M.; El-Masry, E.I., "Tunable matching networks for future MEMS-based transceivers," in *Circuits and Systems, 2004. ISCAS '04. Proceedings of the 2004 International Symposium on* , vol.4, no., pp.IV-457-60 Vol.4, 23-26 May 2004.

[3] Tornatta, P.A.; Gaddi, R., "Aperture tuned antennas for 3G-4G applications using MEMS digital variable capacitor," in *Microwave Symposium Digest (IMS), 2013 IEEE MTT-S International* , vol., no., pp.1-4, 2-7 June 2013

[4] Chen, L.-Y.V.; Forse, R.; Chase, D.; York, R.A., "Analog tunable matching network using integrated thin-film BST capacitors," in *Microwave Symposium Digest, 2004 IEEE MTT-S International* , vol.1, no., pp.261-264 Vol.1, 6-11 June 2004.

[5] van Bezooijen, A.; de Jongh, M.A.; Chanlo, C.; Ruijs, L.; van Straten, F.; Mahmoudi, R.; van Roermund, A.H.M., "A GSM/EDGE/WCDMA Adaptive Series-LC Matching Network Using RF-MEMS Switches," in *Solid-State Circuits, IEEE Journal of* , vol.43, no.10, pp.2259-2268, Oct. 2008.

[6] www.psemi.com/pdf/Psemi_Tuning.pd.

[7] van Bezooijen, A.; Mahmoudi, R.; van Roermund, A.H.M., "Adaptive methods to preserve power amplifier linearity under antenna mismatch conditions," in *Circuits and Systems I: Regular Papers, IEEE Transactions on* , vol.52, no.10, pp.2101-2108, Oct. 2005.

[8] Qizheng Gu, *RF System Design of Transceivers for Wireless Communications*, Springer, New York, 2005.

[9] de Mingo, J.; Valdovinos, A.; Crespo, A.; Navarro, D.; Garcia, P., "An RF electronically controlled impedance tuning network design and its application to an antenna input impedance automatic matching system," in *Microwave Theory and Techniques, IEEE Transactions on* , vol.52, no.2, pp.489-497, Feb. 2004.

[10] Thompson, M.; Fidler, J.K., "Determination of the impedance matching domain of impedance matching networks," in *Circuits and Systems I: Regular Papers, IEEE Transactions on*, vol.51, no.10, pp.2098-2106, Oct. 2004.

[11] Yichuang Sun; Fidler, J.K., "Component value ranges of tunable impedance matching networks in RF communications systems," in HF Radio Systems and Techniques, Seventh International Conference on (Conf. Publ. No. 441) , vol., no., pp.185-189, 7-10 Jul 1997.

[12] Sun, Y.; Fidler, J.K., "Design method for impedance matching networks," in *Circuits, Devices and Systems, IEE Proceedings* - , vol.143, no.4, pp.186-194, Aug 1996.

[13] Qizheng Gu; De Luis, J.R.; Morris, A.S.; Hilbert, J., "An Analytical Algorithm for Pi-Network Impedance Tuners," in *Circuits and Systems I: Regular Papers, IEEE Transactions on* , vol.58, no.12, pp.2894-2905, Dec. 2011.

[14] Qizheng Gu; Morris, A.S., "A New Method for Matching Network Adaptive Control," in *Microwave Theory and Techniques, IEEE Transactions on* , vol.61, no.1, pp.587-595, Jan. 2013.

[15] Ranta, T.; Whatley, R.; Cheng, C.-C.; Facchini, M., "Next-generation CMOS-on-insulator multi-element network for broadband antenna tuning," in *Microwave Conference (EuMC), 2013 European* , vol., no., pp.1567-1570, 6-10 Oct. 2013.

[16] Lagutere, T.; Tahmi, C.; Russat, J., "High-Accuracy Gain and Phase Regulation System for Real Time Compensation," in *Industrial Electronics, 2006.*

[17] http://www.wetterlin.org/sam/PhaseShift_AD8302.pdf.

[18] Reema Sidhwani, "Antenna Tuning for WCDMA RF Front End", M.S. thesis, Dept., Electrical Engineering, Aalto University, 2012.

[19] Müllner, R.; Ball, C.F.; Ivanov, K.; Lienhart, J.; Hric, P., "Contrasting Open-Loop and Closed-Loop Power Control Performance in UTRAN LTE Uplink by UE Trace Analysis," in *Communications, 2009. ICC '09. IEEE International Conference on* , vol., no., pp.1-6, 14-18 June 2009.

[20] Martinez, F.J.O.; Gonzalez, J.S.; Stojmenovic, I., "A parallel hill climbing algorithm for pushing dependent data in clients-providers-servers systems," in*Computers and Communications, 2002. Proceedings. ISCC 2002. Seventh International Symposium on* , vol., no., pp.611-616, 2002.

[21] Jisong Yang; Tao Huang, "Extraction algorithm of reflection coefficient for antenna VSWR meter based on directional coupler and integrated amplitude phase detector," in Cross Strait Quad-Regional Radio Science and Wireless Technology Conference (CSQRWC), 2011 , vol.2, no., pp.1129-1133, 26-30 July 2011.

Appendix A

A Detailed representation for each branch in pi tuner in Chapter 3

C1 Branch (A.1)

$$YC1 = GC1 + I \cdot BC1 = 2 \cdot \mathrm{PI} \cdot f \cdot C1 \cdot \left(\frac{1}{QC1(f)} + I \right)$$

$$GC1 = \frac{2 \cdot \mathrm{PI} \cdot f \cdot C1}{QC1(f)}$$

$$BC1 = 2 \cdot \mathrm{PI} \cdot f \cdot C1$$

C2 Branch (A.2)

$$YC2 = GC2 + I \cdot BC2 = 2 \cdot \mathrm{PI} \cdot f \cdot C2 \cdot \left(\frac{1}{QC2(f)} + I \right)$$

$$GC2 = \frac{2 \cdot \mathrm{PI} \cdot f \cdot C2}{QC2(f)}$$

$$BC2 = 2 \cdot \mathrm{PI} \cdot f \cdot C2 \cdot$$

C3 Branch (A.3)

$$YC3 = GC3 + I \cdot BC3 = 2 \cdot \mathrm{PI} \cdot f \cdot C3 \cdot \left(\frac{1}{QC3(f)} + I \right)$$

$$GC3 = \frac{2 \cdot \mathrm{PI} \cdot f \cdot C3}{QC3(f)}$$

$$BC3 = 2 \cdot \mathrm{PI} \cdot f \cdot C3$$

$$ZC3 = \frac{1}{YC3} = \frac{1}{GC3 + I \cdot BC3}$$

$$ZC3 = RC3 + I \cdot XC3 = \frac{GC3}{BC3^2 + GC3^2} - \frac{\mathrm{I}\,BC3}{BC3^2 + GC3^2}$$

L1 Branch (A.4)

$$ZL1 = RL1 + I \cdot XL1 = 2 \cdot \mathrm{PI} \cdot f \cdot L1 \cdot \left(\frac{1}{QL1(f)} + I \right)$$

$$RL1 = \frac{2 \cdot \mathrm{PI} \cdot f \cdot L1}{QL1(f)}$$

$$XL1 = 2 \cdot \mathrm{PI} \cdot f \cdot L1$$

$$YL1 = \frac{1}{ZL1} = \frac{1}{RL1 + I \cdot XL1} = \frac{RL1}{RL1^2 + XL1^2} - \frac{\mathrm{I}\, XL1}{RL1^2 + XL1^2}$$

$$YL1 = GL1 + I \cdot BL1 = \frac{RL1}{RL1^2 + XL1^2} - \frac{\mathrm{I}\, XL1}{RL1^2 + XL1^2}$$

L2 Branch (A.5)

$$ZL2 = RL2 + I \cdot XL2 = 2 \cdot \mathrm{PI} \cdot f \cdot L2 \cdot \left(\frac{1}{QL2(f)} + I \right)$$

$$RL2 = \frac{2 \cdot \mathrm{PI} \cdot f \cdot L2}{QL2(f)}$$

$$XL2 = 2 \cdot \mathrm{PI} \cdot f \cdot L1$$

$$YL2 = \frac{1}{ZL2} = \frac{1}{RL2 + I \cdot XL2} = \frac{RL2}{RL2^2 + XL2^2} - \frac{\mathrm{I}\, XL2}{RL2^2 + XL2^2}$$

$$YL2 = GL2 + I \cdot BL2 = \frac{RL2}{RL2^2 + XL2^2} - \frac{\mathrm{I}\, XL2}{RL2^2 + XL2^2}$$

L3 Branch (A.6)

$$ZL3 = RL3 + I \cdot XL3 = 2 \cdot \mathrm{PI} \cdot f \cdot L3 \cdot \left(\frac{1}{QL3(f)} + I \right)$$

$$RL3 = \frac{2 \cdot \mathrm{PI} \cdot f \cdot L3}{QL3(f)}$$

$$XL3 = 2 \cdot \mathrm{PI} \cdot f \cdot L3$$

ZL Branch (A.1)

$$ZL = RL + I \cdot XL$$

$$YL = \frac{1}{ZL} = \frac{1}{RL + I \cdot XL} = \frac{RL}{RL^2 + XL^2} - \frac{\mathrm{I}\, XL}{RL^2 + XL^2}$$

$$YL = GL + I \cdot BL = \frac{RL}{RL^2 + XL^2} - \frac{\mathrm{I}\, XL}{RL^2 + XL^2}$$

Zo Branch (A.7)

$$Zo = Ro + I \cdot Xo$$

$$Yo = Go + I \cdot Bo = \frac{Ro}{Ro^2 + Xo^2} - \frac{\mathrm{I}\, Xo}{Ro^2 + Xo^2}$$

Appendix B

B Output of Hill Climbing Algorithm in Chapter 4

B.1 Convergence after 16 Iterations

```
Initial voltage A/B/C : 4V
Tune step voltage: 1,,,,,,,
-------------------------------------Iteration : 0,,,,,,,
Voltage Tune Step: 5,,,,,,,
0,,,,3.95,3.95,3.95,-1.72
1,,,,4.89,4.89,4.89,-2.06
2,,,,4.89,4.89,3.95,-2.14
3,,,,4.89,3.95,4.89,-1.72
4,,,,4.89,3.95,3.95,-1.89
5,,,,3.95,4.89,4.89,-1.89
6,,,,3.95,4.89,3.95,-1.89
7,,,,3.95,3.95,4.89,-1.72
8,,,,3.95,3.95,3.95,-1.72
Minimum Point from Scan: 2,,,,,,,
Magitude (dB): -2.14,,,,,,,
-------------------------------------Iteration : 1,,,,,,,
Voltage Tune Step: 5,,,,,,,
0,,,,4.89,4.89,3.95,-1.97
1,,,,5.83,5.83,3.95,-2.56
2,,,,5.83,5.83,3.95,-2.56
3,,,,5.83,3.95,3.95,-1.89
4,,,,5.83,3.95,3.95,-1.89
5,,,,3.95,5.83,3.95,-2.06
6,,,,3.95,5.83,3.95,-2.06
7,,,,3.95,3.95,3.95,-1.64
8,,,,3.95,3.95,3.95,-1.64
Minimum Point from Scan: 1,,,,,,,
Magitude (dB): -2.56,,,,,,,
```

No. 0 : initial point

No. 1-8: candidates

Minimum point among candidates

Minimum point from previous iteration is now the initial point = No. 0

```
-------------------------------------Iteration : 15,,,,,,,
Voltage Tune Step: 5,,,,,,,
0,,,,18.05,16.17,3.95,-9.48
1,,,,18.99,17.11,3.95,-9.65
2,,,,18.99,17.11,3.95,-9.65
3,,,,18.99,15.23,3.95,-9.65
4,,,,18.99,15.23,3.95,-9.65
5,,,,17.11,17.11,3.95,-9.31
6,,,,17.11,17.11,3.95,-9.31
7,,,,17.11,15.23,3.95,-9.31
8,,,,17.11,15.23,3.95,-9.31
Minimum Point from Scan: 1,,,,,,,
Magitude (dB): -9.65,,,,,,,
-------------------------------------Iteration : 16,,,,,,,
Voltage Tune Step: 5,,,,,,,
0,,,,18.99,17.11,3.95,-9.65
1,,,,19.93,18.05,4.89,-9.73
2,,,,19.93,18.05,3.95,-10.06
3,,,,19.93,16.17,4.89,-9.73
4,,,,19.93,16.17,3.95,-10.06
5,,,,18.05,18.05,4.89,-9.4
6,,,,18.05,18.05,3.95,-9.73
7,,,,18.05,16.17,4.89,-9.56
8,,,,18.05,16.17,3.95,-9.9
Minimum Point from Scan: 2,,,,,,,
Magitude (dB): -10.06,,,,,,,
Converged into VSWR < 2 ,,,,,,,
```

Solution converged into <-10 dB

B.2 Unstable Convergence

```
-------------------------------------Iteration : 14,,,,,,,
Voltage Tune Step: 5,,,,,,,
0,,,,,16.17,3.95,-9.73
1,,,,,17.11,3.95,-9.81
2,,,,,17.11,3.95,-9.9
3,,,,,15.23,3.95,-9.81
4,,,,,15.23,3.95,-9.81
5,,,,,17.11,3.95,-9.48
6,,,,,17.11,3.95,-9.48
7,,,,,15.23,3.95,-9.56
8,,,,,15.23,3.95,-9.56
Minimum Point from Scan: 2,,,,,,,
Magitude (dB): -9.90,,,,,,,
-------------------------------------Iteration : 15,,,,,,,
Voltage Tune Step: 5,,,,,,,
0,,,,,17.11,3.95,-9.9
1,,,,,18.05,3.95,-9.98
2,,,,,18.05,3.95,-9.9
3,,,,,16.17,3.95,-9.98
4,,,,,16.17,3.95,-9.98
5,,,,,18.05,3.95,-9.73
6,,,,,18.05,3.95,-9.65
7,,,,,16.17,3.95,-9.65
8,,,,,16.17,3.95,-9.65
Minimum Point from Scan: 1,,,,,,,
Magitude (dB): -9.98,,,,,,,
-------------------------------------Iteration : 16,,,,,,,
Voltage Tune Step: 5,,,,,,,
0,,,,,18.05,3.95,-10.06
Already converged. ,,,,,,,
-------------------------------------Iteration : 0,,,,,,,
Voltage Tune Step: 5,,,,,,,
0,,,,,18.05,3.95,-10.23
Already converged. ,,,,,,,
-------------------------------------Iteration : 0,,,,,,,
Voltage Tune Step: 5,,,,,,,
0,,,,,18.05,3.95,-10.23
Already converged. ,,,,,,,
-------------------------------------Iteration : 0,,,,,,,
Voltage Tune Step: 5,,,,,,,
0,,,,,18.05,3.95,-9.98
1,,,,,18.99,3.95,-9.9
2,,,,,18.99,3.95,-9.9
3,,,,,17.11,3.95,-9.9
4,,,,,17.11,3.95,-9.98
5,,,,,18.99,3.95,-9.73
6,,,,,18.99,3.95,-9.81
7,,,,,17.11,3.95,-9.81
8,,,,,17.11,3.95,-9.9
Minimum Point from Scan: 0,,,,,,,
Magitude (dB): -9.98,,,,,,,
-------------------------------------Iteration : 1,,,,,,,
Voltage Tune Step: 5,,,,,,,
0,,,,,18.05,3.95,-9.9
1,,,,,18.99,3.95,-9.9
2,,,,,18.99,3.95,-9.98
3,,,,,17.11,3.95,-9.98
4,,,,,17.11,3.95,-10.06
5,,,,,18.99,3.95,-9.73
6,,,,,18.99,3.95,-9.73
7,,,,,17.11,3.95,-9.81
8,,,,,17.11,3.95,-9.81
Minimum Point from Scan: 4,,,,,,,
Magitude (dB): -10.06,,,,,,,
Converged into VSWR < 2 ,,,,,,,
```

B.3 Initial point is already at convergence (<-10dB)

```
-------------------------------------Iteration : 0,,,,,,,
Voltage Tune Step: 5,,,,,,,
0,,,,12.97,12.97,12.97,-13.23
Already converged. ,,,,,,,
-------------------------------------Iteration : 0,,,,,,,
Voltage Tune Step: 5,,,,,,,
0,,,,12.97,12.97,12.97,-13.23
Already converged. ,,,,,,,
```

B.4 Fast convergence after two iterations

```
-------------------------------------Iteration : 0,,,,,,,
Voltage Tune Step: 5,,,,,,,
0,,,,9.96,9.96,9.96,-6.14
1,,,,10.9,10.9,10.9,-9.4
2,,,,10.9,10.9,9.02,-9.98
3,,,,10.9,9.02,10.9,-8.48
4,,,,10.9,9.02,9.02,-9.56
5,,,,9.02,10.9,10.9,-7.31
6,,,,9.02,10.9,9.02,-8.23
7,,,,9.02,9.02,10.9,-7.06
8,,,,9.02,9.02,9.02,-7.98
Minimum Point from Scan: 2,,,,,,,
Magitude (dB): -9.98,,,,,,,
-------------------------------------Iteration : 1,,,,,,,
Voltage Tune Step: 5,,,,,,,
0,,,,10.9,10.9,9.02,-8.9
1,,,,11.84,11.84,9.96,-9.65
2,,,,11.84,11.84,8.08,-10.15
3,,,,11.84,9.96,9.96,-8.9
4,,,,11.84,9.96,8.08,-9.9
5,,,,9.96,11.84,9.96,-7.73
6,,,,9.96,11.84,8.08,-8.56
7,,,,9.96,9.96,9.96,-7.56
8,,,,9.96,9.96,8.08,-8.48
Minimum Point from Scan: 2,,,,,,,
Magitude (dB): -10.15,,,,,,,
Converged into VSWR < 2 ,,,,,,,
```

Appendix C

C S11 Measurement Characterization in Section 5.2

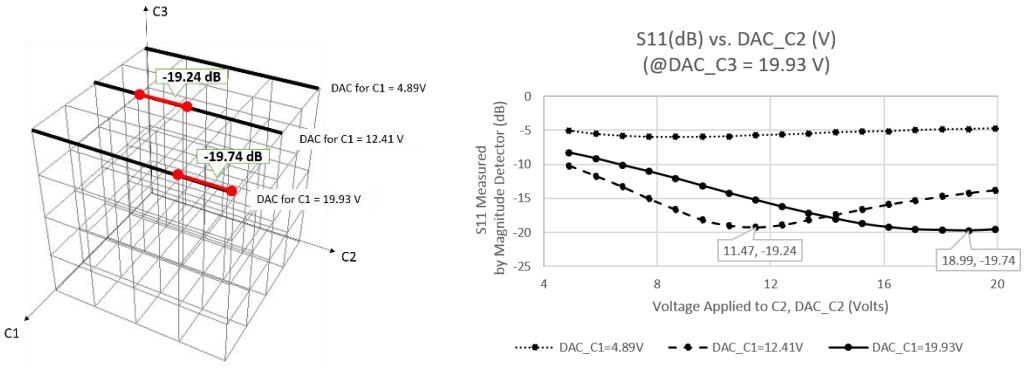

(a) XY plane at C2-direction (C3=19.93V)

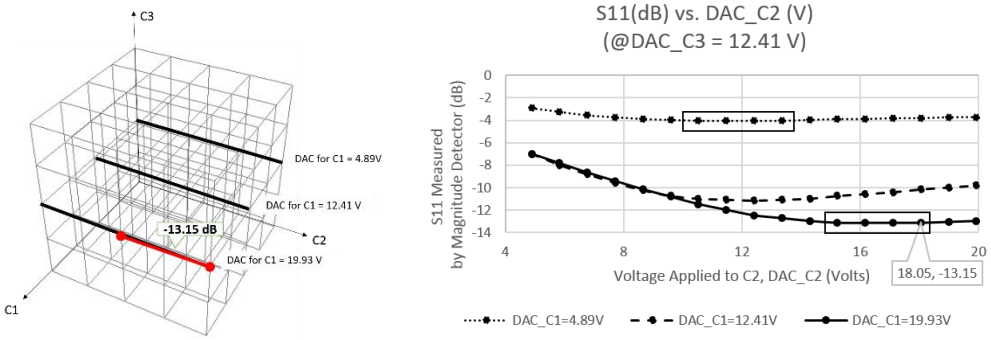

(b) XY plane at C2 direction (C3=12.41 V)

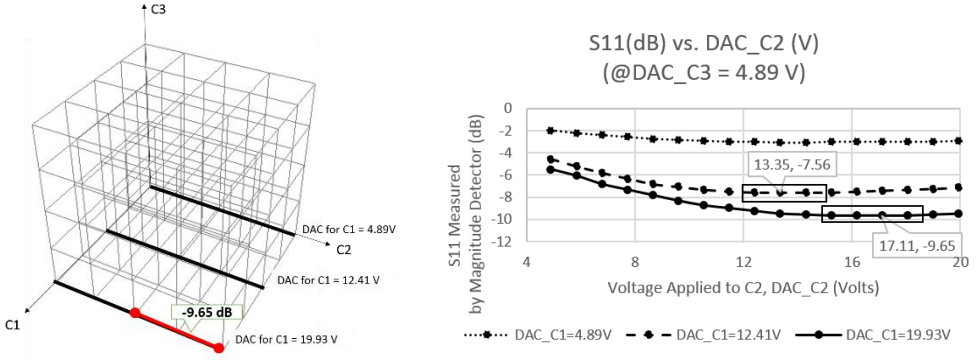

(c) XY plane at C2 direction (C3=4.89 V)

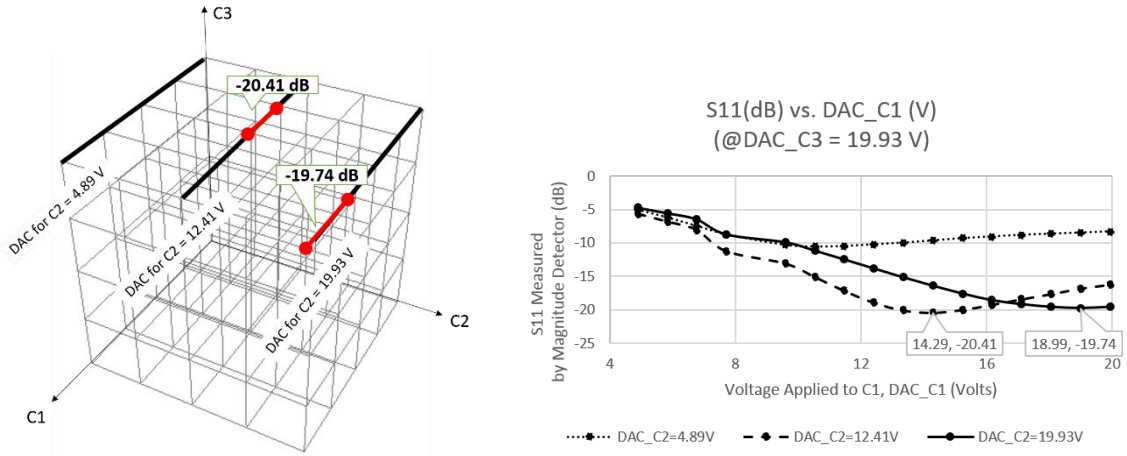

(d) XY plane at C1 direction (C3=19.93 V)

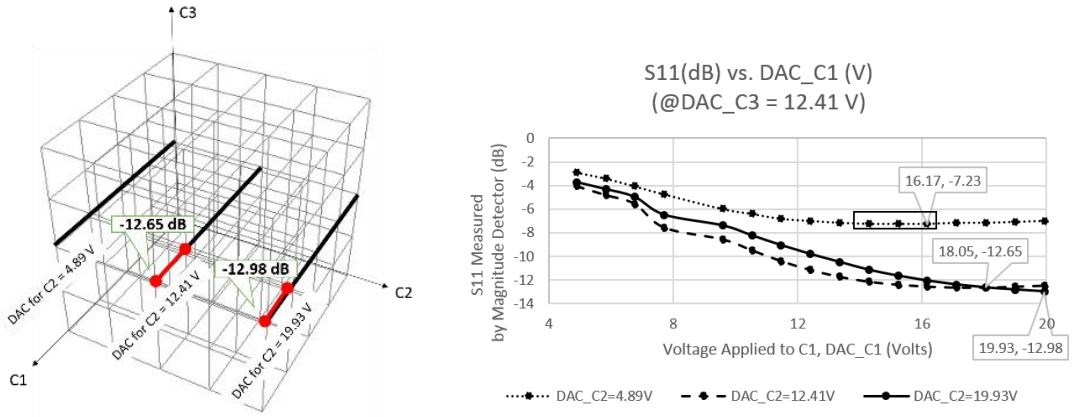

(e) XY plane at C1 direction (C3=12.41V)

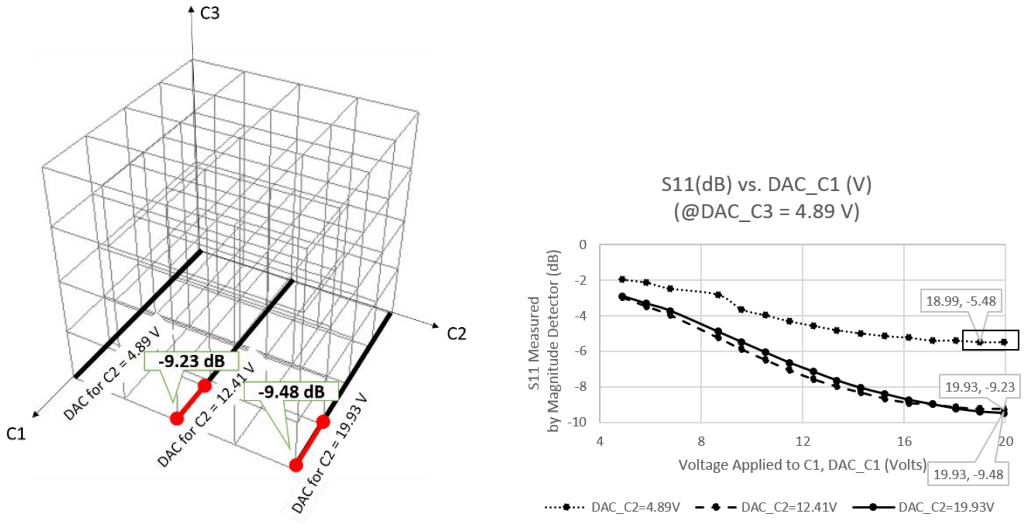

(f) XY plane at C1 direction (C3=4.89 V)